European Journal of Medicinal Chemistry 297 (2025) 117983

Contents lists available at ScienceDirect

European Journal of Medicinal Chemistry

journal homepage: www.elsevier.com/locate/ejmech

Research paper

Design, synthesis, and biological activity of 2-aroylbenzofuran-3-ols and 2-aroylbenzofuran derivatives: A new route towards *h*MAO-B inhibition

Paolo Guglielmi [a,1], Michele Coluccia [a,1], Guya Diletta Marconi [b], Francesco Ortuso [c,d], Francesca Procopio [c], Simone Carradori [e], Jacopo Pizzicannella [b], Francesca Arrighi [a], Anna Troiani [a], Chiara Salvitti [a], Fernanda Borges [f,g], Daniel Chavarria [h], Paola Chimenti [a,*], Daniela Secci [a,**], Francesca Diomede [b]

[a] Department of Drug Chemistry and Technologies, Sapienza University of Rome, Rome, Italy
[b] Department of Innovative Technologies in Medicine & Dentistry, "G. d'Annunzio" University of Chieti-Pescara, Chieti, Italy
[c] Department of Health Sciences, University "Magna Graecia" of Catanzaro, Campus Universitario "S. Venuta", Catanzaro, Italy
[d] Net4Science Academic Spin-Off, Università "Magna Græcia" di Catanzaro, Campus "S. Venuta", Catanzaro, Italy
[e] Department of Pharmacy, "G. d'Annunzio" University of Chieti-Pescara, Chieti, Italy
[f] MedInUP, Center for Drug Discovery and Innovative Medicines, University of Porto, Porto, Portugal
[g] Department of Chemistry and Biochemistry, Faculty of Sciences/Department of Biomedicine, Pharmacology and Therapeutics Unit, Faculty of Medicine, University of Porto, Porto, Portugal
[h] CIQUP-IMS, Department of Chemistry and Biochemistry, Faculty of Sciences, University of Porto, Porto, Portugal

ARTICLE INFO

Keywords:
Human monoamine oxidase (*h*MAO)
*h*MAO-B selective inhibitors
2-aroylbenzofurans
Neurodegenerative diseases
Parkinson's disease

ABSTRACT

The crucial role of human monoamine oxidases (*h*MAOs), particularly the B isoform, in the pathogenesis of neurodegenerative diseases has been extensively studied. Alongside numerous other factors, the clinical use of *h*MAO-B inhibitors to alleviate symptoms of Parkinson's disease is well-established. In order to develop novel *h*MAO-B inhibitors as potential candidates for the treatment of these conditions, we have designed and synthesized two libraries of compounds based on the 2-aroylbenzofuran-3-ol and the 2-aroylbenzofuran scaffolds. The *h*MAO inhibitory activity and selectivity of these compounds was thoroughly investigated. In general, the 2-aroylbenzofuran-3-ols were unable to inhibit *h*MAO isoforms. In contrast, 2-aroylbenzofuran derivatives acted as potent and selective *h*MAO-B inhibitors, showing IC_{50} values within the nanomolar range and as low as 8.2 nM. The best compounds exhibited broad safety ranges in human gingival fibroblasts (hGFs) and SH-SY5Y neuroblastoma cells. A preliminary evaluation of the compounds' neuroprotective effects was conducted through the co-exposure of the cells to the neurotoxic agent 6-hydroxydopamine (6-OHDA) and the synthesized compounds, whose activity was comparable to that of (*R*)-(−)-deprenyl, the reference *h*MAO-B inhibitors. The characterization of the compounds was enriched with the *in silico* prediction of the drug-likeness of the most active compounds among the 2-aroyl benzofurans using the free web tool SwissADME. All compounds were predicted to have high gastrointestinal absorption and to permeate the blood-brain barrier and molecular modelling studies provided insights into the molecular mechanisms responsible for the high *h*MAO-B inhibitory potency and selectivity of 2-aroylbenzofurans.

1. Introduction

Neurodegenerative disorders, whose most well-known representatives are Alzheimer's (AD) and Parkinson's disease (PD), are among the heaviest burdens on the healthcare systems all over the world [1–3]. These conditions are characterized, each through its own peculiar pathogenetic mechanisms—by neuronal loss and the degeneration of behavioural and cognitive functions such as memory and learning. They also involve increased difficulty in movement, leading to a deterioration in patients' quality of life and an overall degeneration of the central

* Corresponding author.
** Corresponding author.
E-mail addresses: paola.chimenti@uniroma1.it (P. Chimenti), daniela.secci@uniroma1.it (D. Secci).
[1] These authors contributed equally to the work.

https://doi.org/10.1016/j.ejmech.2025.117983
Received 13 May 2025; Received in revised form 15 July 2025; Accepted 16 July 2025
Available online 18 July 2025

nervous system [4,5]. Although AD and PD are caused by two very distinct pathogenetic mechanisms, it is possible to identify common molecular pathways that play a pivotal role in the development and worsening of both pathologies [6]. One of these is the involvement of monoamine neurotransmitters and their metabolism in the brain by human monoamine oxidases (MAOs), the main enzymes implicated in their metabolic transformation [7]. Monoamine neurotransmitters, such as dopamine (DA), serotonin (5-HT), and norepinephrine (NE), are essential to brain development and synaptic transmission. Furthermore, monoamines, which have important neuromodulatory activities, play a fundamental role in cognitive functions like memory and learning. Hence, an enhancement of monoaminergic neurotransmission could significantly improve the conditions of patients with AD and PD [8].

Monoamine oxidases are flavine adenine dinucleotide (FAD)-containing enzymes located at the outer mitochondrial membrane and deputed to the catabolism of monoamines through oxidative deamination [9]. There are two isoforms of MAO in humans: *h*MAO-A and *h*MAO-B, each with a proper tissue and organ distribution as well as substrate specificity, although both enzymes are involved in the metabolism of common substrates, like dopamine [10]. Thanks to an aromatic cage formed by tyrosine residues, MAOs draw the substrate near to the flavin cofactor, obtaining the oxidation of the amine into the corresponding imine, which is then non-enzymatically hydrolysed into an aldehyde [11]. The regeneration of the oxidized cofactor consumes molecular oxygen and produces hydrogen peroxide (H_2O_2) [12,13]. While H_2O_2 is typically detoxified within cells by glutathione peroxidase and catalase, enhanced *h*MAO-driven H_2O_2 production has been observed with aging and in several age-related diseases, including AD and PD [14]. Particularly, *h*MAO-B expression drastically decreases after a first expression peak during early childhood; however, its activity starts to increase again in elderly people [15,16]. This may result in an increase in the production of oxidant species like hydrogen peroxide, which contribute to lipid peroxidation, free radicals' generation, and the involution of the nervous tissue [17,18]. In 1999, Alper and colleagues linked the increased *h*MAOs activity and subsequent H_2O_2-driven oxidative stress to neurological disorders, thus pointing out *h*MAOs as potential factor involved in these age-associated diseases [19].

In PD, the increased activity of *h*MAO-B in glial cells leads to enhanced DA metabolism, which not only depletes neurotransmitter reserves in the central nervous system (CNS) but also leads to the accumulation of neurotoxic molecules including H_2O_2, 3,4-dihydroxyphenylacetaldehyde (DOPAL), and ammonia [20,21]. DOPAL, the aldehyde derived from the oxidative deamination of dopamine, can be converted through oxidation into its corresponding quinone [22,23]. Both compounds seem to stimulate the oligomerization of α-synuclein, whose aggregates are the primary components of Lewy bodies, intracytoplasmic inclusions characteristic of Parkinson's affected brains and responsible, through cell-to-cell migration, for the neurodegeneration spread in the brain [24]. DOPAL accumulation can also originate from the inhibition of aldehyde dehydrogenase (ALDH), the enzyme that converts DOPAL to 3,4-dihydroxyphenylacetic acid (DOPAC), because of lipid peroxidation products generated by H_2O_2 [25]. The H_2O_2-driven lipid peroxidation can also prompt α-synuclein aggregation, thus contributing to the motor deficits of PD [26,27]. In addition to lipid peroxidation, H_2O_2 takes part in several harmful processes. Indeed, once produced in glial cells, H_2O_2 can diffuse into nigrostriatal DA neurons, where it participates along with ferrous ion (Fe^{2+}) in the Fenton reaction to afford oxygen radicals contributing to DA neuronal death [15,28]. Moreover, H_2O_2-driven oxidative stress has been related to mitochondrial dysfunction, contributing to DA neuron death [29,30].

In light of the above, MAO-B inhibitors have been widely studied and are clinically used in the treatment of PD [31–35]. To date, three *h*MAO-B inhibitors have been approved: two irreversible (selegiline and rasagiline) and one reversible (safinamide) inhibitors [34,36]. The need for selective *h*MAO-B inhibitors comes from the unpleasant adverse effects that results from the simultaneous administration of non-selective *h*MAO inhibitors and the ingestion, through the diet, of tyramine or other sympathomimetic monoamines-rich foods, like cheese and chocolate. This occurrence, called "cheese effect", leads to the stimulation of the sympathetic nervous system, resulting in hypertensive crisis and other cardiovascular symptoms [37]. On the basis of these considerations, in 2019 we developed the benzo[*b*]thiophen-3-ole fragment as a valuable scaffold for the development of potent and selective *h*MAO-B inhibitors [38]. Most of the derivatives inhibited this isoform, presenting IC_{50} values in micromolar/sub-micromolar range. Moreover, the most active compounds were investigated in an *ex vivo model* of rat cortex synaptosomes in both basal and LPS-induced inflammatory conditions, resulting to exert protective effects.

Continuing our efforts in the development of *h*MAO-B inhibitors, we report here the design and synthesis of two distinct scaffolds, 2-aroylbenzofuran-3-ol and 2-aroylbenzofuran, derived from structural modifications of the benzo[*b*]thiophen-3-ol core aimed at optimizing MAO inhibitory activity. The compounds exhibiting the most potent *h*MAOs inhibition have been characterized at cellular level to assess their cytotoxicity against two different cell lines (SH-SY5Y and hGF); moreover, the ones exhibiting the best toxicological profile were further evaluated for their neuroprotective activity in cellular Parkinson's model (SH-SY5Y treated with 6-hydroxydopamine, 6-OHDA). Finally, the characterization of the compounds was complemented by *in silico* prediction of the drug-likeness of the most active 2-aroylbenzofurans using the free web-based tool SwissADME.

1.1. Design of the novel inhibitors

The design of the novel MAOs inhibitors initiated from the isosteric replacement of the benzothiophene's sulfur atom with an oxygen to obtain the corresponding benzofuran analogues (Fig. 1, Library 1). The S/O isosteric replacement, but also the *vice versa* (O/S), has been extensively exploited on different scaffolds such as chromones and coumarins to obtain potent and selective MAOs inhibitors [39]. Unfortunately, the benzofuran-3-ol derivatives obtained from this approach (Fig. 1, Library 1) were devoid of significant *h*MAO inhibitory activity ($IC_{50} > 10$ μM, see *section 2.3.1*). So, we tried a further structural modification based on the removal of the hydroxyl group placed at the position 3 of the benzofuran ring. Interestingly, the so obtained 2-aroyl benzofuran scaffold shares some important molecular features with chromone, coumarin and chalcone, three molecular skeletons extensively exploited for the development of MAO inhibitors (Fig. 1, Library 2) [40–42]. Indeed, the 2-aroyl benzofuran core formally results from (i) "endocyclic" to "exocyclic" carbonyl displacement of either the coumarin or chromone rings with the simultaneous pyran-2/4-one rings contraction to obtain the furan core and (ii) cyclization of the chalcone structure on the α-carbon of the Michael system (Fig. 1). These derivatives (Library 2) exhibited improved results demonstrating potent and selective activity against *h*MAO-B, with respect to the related benzofuran-3-ol derivatives (Library 1) (see *section 2.3.1*).

2. Results and discussion

2.1. Chemistry

For the synthesis of the 2-aroylbenzofuran-3-ols (Library 1, compounds **1**–**10**) we employed a microwave-assisted reaction between methylsalicylate and the proper α-bromoacetophenone (Scheme 1a). The reactions were performed at 100 °C in acetone, for 15 min using potassium phosphate as base [43]. The 2-aroyl benzofuran derivatives (Library 2, compounds **11**–**21**) were obtained by reacting salicylaldehyde with the proper α-bromoacetophenone in refluxing acetonitrile (CH_3CN) using potassium carbonate (K_2CO_3) as base (Scheme 1b) [44]. The synthesized compounds were purified through crystallization and/or chromatographic methods and obtained in moderate to high yields. They were all structurally characterized through ^{1}H NMR, ^{13}C

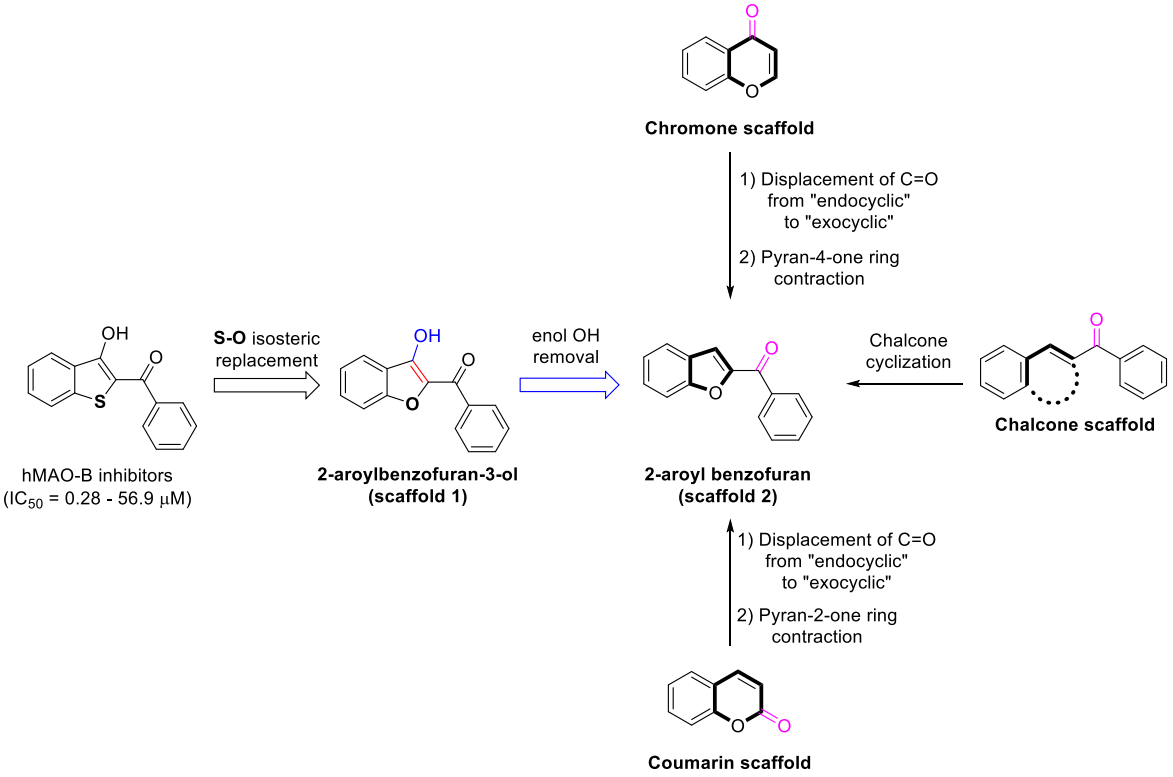

Fig. 1. Design and development of the benzofuran-based scaffold.

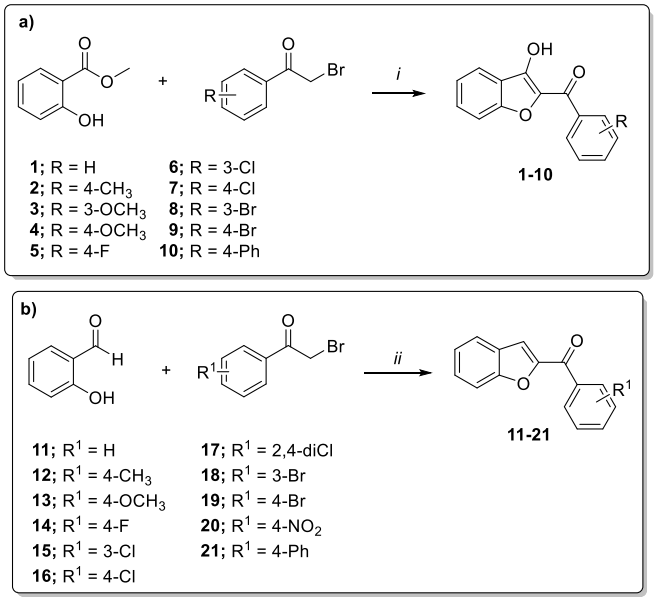

Scheme 1. a) Synthesis of the 2-aroylbenzofuran-3-ols **1**–**10**. **b)** Synthesis of the 2-aroyl benzofuran derivatives **11**–**21**. Reagents and conditions: (*i*) K_3PO_4, acetone, 100 °C (MW), 15 min (yields = 43–62 %); (*ii*) K_2CO_3, acetonitrile, reflux, 6–12h (yields = 39–57 %).

NMR and HRMS before their evaluation in the *in vitro* assays and their NMR-purity was higher than 95 % (further details concerning the synthetic procedures, yields, ^{1}H NMR/^{13}C NMR and HRMS spectra are reported in the material and methods section and/or supporting information file).

2.2. Biology

2.2.1. Monoamine oxidase inhibitory activity

The inhibitory activity of the compounds has been tested against both *h*MAO-A and *h*MAO-B using a spectrophotometric assay based on the conversion rate of kynuramine, a substrate of both MAO enzymes, into 4-hydroxyquinoline, its corresponding oxidized metabolite. The inhibitory activities of compounds **1**–**21** are summarized in Table 1 along with selectivity index (SI) values given as the ratio (IC_{50} *h*MAO-A)/(IC_{50} *h*MAO-B). Compounds were initially screened at a fixed concentration of 10 μM to identify those capable of achieving at least 50 % inhibition. Only compounds meeting this threshold were subsequently selected for IC_{50} determination. The two sub-series of developed compounds showed very different *h*MAO inhibition profiles when tested *in vitro*. In general, compounds **1**–**10**, characterized by the presence of a hydroxyl group in position 3 on the benzofuran structure, did not display significant *h*MAO inhibitory activities (IC_{50} > 10 μM). The only exception was the derivative **6,** endowed with *meta*-chloro substituted phenyl ring, which presented an IC_{50} of 4.1 μM against the isoform B. As mentioned above, the benzofuran-3-ol scaffold was developed starting from a library of benzo[*b*]thiophen-3-ol compounds previously described by our group [38]. The data presented here demonstrate that the isosteric replacement of the sulfur atom with the oxygen in this scaffold is not tolerated, leading to a significant reduction in both inhibitory activity and selectivity against MAO-B. In order to evaluate the role of the hydroxyl group in position 3 of the benzofuran ring on the activity loss, we decided to maintain the isosteric oxygen atom of the benzofuran structure while eliminating the 3-hydroxyl group. Indeed, the active site of isoform B, as has been widely described, is characterized by the presence of several lipophilic residues which are essential for the stabilization and proper orientation of substrates and inhibitors [10].

Therefore, the lack of MAO-B inhibitory activity and selectivity of benzofuran-3-ol derivatives may be due to the increased hydrophilicity and the steric hindrance provided by the 3-hydroxyl group. As a matter

Table 1
Inhibitory activity (IC_{50}) and selectivity index (SI) of compounds **1**–**21** towards *h*MAO-A and *h*MAO-B.

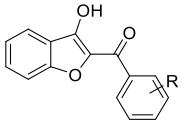

Compound	R	IC_{50} ± SD (μM)[a]		SI [b]
		*h*MAO-A	*h*MAO-B	
1	H	>10 (0 %) [c]	>10 (0.4 %) [c]	NA [d]
2	4-CH_3	>10 (0 %) [c]	>10 (40.7 %) [c]	NA [d]
3	3-OCH_3	>10 (0 %) [c]	>10 (25.0 %) [c]	NA [d]
4	4-OCH_3	>10 (0 %) [c]	>10 (35.9 %) [c]	NA [d]
5	4-F	>10 (0 %) [c]	>10 (0 %) [c]	NA [d]
6	3-Cl	>10 (0 %) [c]	4.0835 ± 0.5234	>2.4
7	4-Cl	>10 (43.5 %) [c]	>10 (29.8 %) [c]	NA [d]
8	3-Br	>10 (0 %) [c]	>10 (47.6 %) [c]	NA [d]
9	4-Br	>10 (0 %) [c]	>10 (10.5 %) [c]	NA [d]
10	4-Ph	>10 (0 %) [c]	>10 (32.7 %) [c]	NA [d]
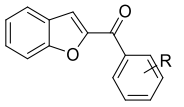				
11	H	9.0420 ± 1.7801	0.2117 ± 0.0223	43.4
12	4-CH_3	5.1064 ± 0.2941	0.0121 ± 0.0004	422.0
13	4-OCH_3	5.5852 ± 0.8187	0.0085 ± 0.0007	626.3
14	4-F	>10 (45.8 %) [c]	0.2296 ± 0.0127	>43.7 [e]
15	3-Cl	3.4923 ± 0.2313	0.0188 ± 0.0003	186.6
16	4-Cl	7.2054 ± 0.2243	0.0268 ± 0.0016	268.8
17	2,4-diCl	7.2176 ± 0.9568	0.591 ± 0.0986	12.2
18	3-Br	6.4293 ± 0.4828	0.0135 ± 0.0009	494.6
19	4-Br	6.0640 ± 0.6323	0.0166 ± 0.0006	356.5
20	4-NO_2	>10 (41.1 %) [c]	0.0082 ± 0.0008	>1221.0 [e]
21	4-Ph	>10 (13.2 %) [c]	0.1357 ± 0.0099	>73.7 [e]
(*R*)-(−)-Deprenyl		>10 (21.2 %) [c]	0.0414 ± 0.0057	>244.0 [e]
Clorgyline		0.0023 ± 0.0009	3.32 ± 0.4235	0.00069

[a] Values are the mean ± SD of triplicate determinations.
[b] Selectivity index for the MAO-B isoform, given as the ratio: (IC_{50} MAO-A)/(IC_{50} MAO-B).
[c] The values in brackets indicate the percentage of inhibition observed during the initial screening at a fixed concentration of 10 μM.
[d] Not assessable.
[e] Values obtained assuming that the corresponding IC_{50} value against hMAO-A is the highest concentration tested (10 μM).

of fact, the non-hydroxylated compounds **11**–**21** were potent and selective *h*MAO-B inhibitors, showing IC_{50} values within the nanomolar range. Indeed, if compared with the non-substituted compound **11** (*h*MAO-B IC_{50} = 0.217 μM), the introduction of any of the selected functional groups generally enhanced the compounds' inhibitory activity towards *h*MAO-B, with the only exceptions being the *para*-F (**14**) and 2,4-dichloro (**17**) derivatives. The incorporation of a *para*-fluorine atom (**14**) maintained the inhibitory activity against *h*MAO-B (**14**, *h*MAO-B IC_{50} = 0.229 μM), while reducing the affinity for *h*MAO-A (IC_{50} > 10 μM). In contrast, the presence of the 2,4-dichloro substitution reduced the compound's *h*MAO-B inhibitory activity and selectivity (compound **17**, IC_{50} MAO-B = 0.591 μM; SI = 12.2). The 2-aroyl benzofuran derivative containing a *para*-nitro group (compound **20**) stood out as the most potent and selective compound of the series, showing a *h*MAO-B IC_{50} value of 8.2 nM while being inactive towards the isoform A (SI > 1221.0). Compound **13**, which contains a *para*-methoxy substituent, also acted as a potent *h*MAO-B inhibitor (*h*MAO-B IC_{50} = 8.5 nM). However, it was less selective than compound 20 since it also displayed moderate *h*MAO-A inhibitory activity (IC_{50} *h*MAO-A = 5.6 μM; SI = 626.3). The introduction of a *para*-methyl group (compound **12**), still led to a noteworthy *h*MAO-B IC_{50} of 12.1 nM, similar to the value observed for the *para*-methoxy substituted compound (**13**). The presence of this weak electron-withdrawing substituent slightly improved the affinity against *h*MAO-A (**12**, IC_{50} *h*MAO-A = 5.1 μM; SI = 422). As a result of the slight increases in the IC_{50} value against MAO-B and the decreased IC_{50} value against *h*MAO-A, a further reduction in the selectivity of compound **12** was observed (**12**, SI = 422). Similar to what was observed in our previous study [38], the halogen-substituted compounds exhibited a trend for the inhibitory activity data (Table 1). In particular, by analysing the IC_{50} values of the compounds bearing halogen in the *para* position of the phenyl ring, it is possible to note that IC_{50} is strongly improved from *para*-F (**14**, IC_{50} *h*MAO-B = 0.229 μM; SI > 43.7) to *para*-Cl (**16**, IC_{50} *h*MAO-B = 0.0268 μM; SI = 268.8) and eventually to *para*-Br (**19**, IC_{50} *h*MAO-B = 0.017 μM; SI = 356.5). These compounds also showed similar trend for the inhibitory activity data of the isoform A, albeit to a lesser extent (Table 1). Indeed, the *h*MAO-B inhibition improvement was greater than that of *h*MAO-A, thus resulting in higher selectivity indexes. The shift of halogen atoms from *para* to *meta* position, observed in compounds **15** (*meta*-Cl) and **18** (*meta*-Br), led to similar *h*MAO-B inhibitory activity if compared with the corresponding *para*-substituted compounds (**16** and **19**, respectively). However, the presence of a *meta*-chloro in compound **15** slightly enhanced the inhibitory against *h*MAO-A, resulting in a reduced SI of 186.6. Interestingly, the introduction of an additional halogen on the phenyl ring seem to negatively affect isoform B inhibition, as demonstrated by compound **17** bearing a 2,4-dichloro substitution and endowed with sub-micromolar IC_{50} against hMAO-B. The insertion of larger substituents resulted in decreased inhibition activity. In fact, compound **21**, with 4-phenyl substitution, showed a more than ten-fold weaker *h*MAO-B inhibition (**21**, IC_{50} *h*MAO-B = 0.136 μM) compared with the related 4-methyl and 4-methoxyl compounds. Finally, compared with the corresponding 3-hydroxylated compounds, compounds **11**–**21** showed a conspicuous increase both in inhibitory activity and selectivity, also with respect to the benzo[*b*]tiophen-3-ols [38] (ref), with the IC_{50} being, on average, tenfold higher than the benzofurans.

The two most active compounds, derivatives **13** and **20**, were further investigated to evaluate their mechanisms of action (Fig. S2, Supporting Information). This was done by measuring the reaction rate of kynuramine conversion to 4-quinolinol at varying substrate concentrations, both in the presence and absence of the inhibitors. The Michaelis–Menten curves and corresponding Lineweaver–Burk plots indicate that compound **13** exhibits a competitive inhibition mechanism, while compound **20** shows a mixed inhibition mechanism (Fig. S2, Supporting Information).

2.2.2. Cell metabolic activity: effects of hMAO-A and hMAO-B inhibitors on hGFs and on SH-SY5Y cell lines

The inhibitory activity (IC_{50}) and selectivity index (SI) of compounds reported in Table 1 evidenced that derivatives **11**–**21** are potent and selective *h*MAO-B inhibitors. The biological effects on cell viability of derivatives **12**, **13**, **15**, **16**, **18**, **19,** and **20** were evaluated by means of MTS assay, a colorimetric assay used to measure cell viability, proliferation, and cytotoxicity in cultured cells. In particular we investigated the selected compounds on cellular models of human gingival fibroblasts (hGFs) and human neuroblastoma cell line (SH-SY5Y) [45,46]. Compounds **12**, **13**, **15**, **16**, **18**, **19,** and **20** were tested individually and compared to the clinically available MAO-B inhibitor (*R*)-(−)-Deprenyl [47], and to 6-hydroxydopamine (6-OHDA), used as a model to recapitulate the PD, in order to evaluate the effect on cell viability [48,49]. hGFs (Fig. 2) and SH-SY5Y cells (Fig. 3) were incubated for 24 h with the test compounds at concentrations between 12.5 up to 100 μM. None of the tested compounds significantly affected cell viability in both cell lines.

In parallel, compounds **12**, **13**, **15**, **16**, **18**, **19** and **20**, along with (*R*)-(−)-Deprenyl, were evaluated in co-treatment with 500 μM 6-OHDA (based on our previous results, not shown). These compounds mitigated the effects of 6-OHDA alone, resulting in an approximate 10–20 % increase in SH-SY5Y cell viability after 12 h of culture. On the other hand, the same compounds were assessed in co-treatment with 6-OHDA

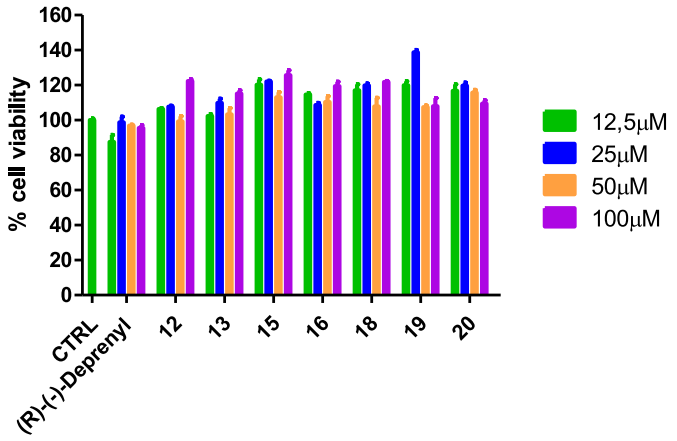

Fig. 2. Cell viability assay. Histograms represent the viability dose-response of hGFs cells exposed to (*R*)-(−)-Deprenyl, and compounds **12**, **13**, **15**, **16**, **18**, **19** and **20** at 12.5 μM, 25 μM, 50 μM and 100 μM for 24 h. Cell viability was evaluated using MTS assay and normalized to control cells treated with DMSO (0.2 % as final concentration). Bars represent means, and the error bars represent the standard deviation.

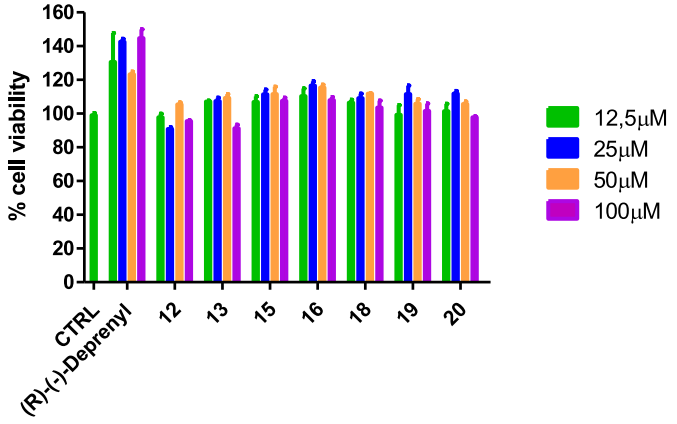

Fig. 3. Cell viability assay. Histograms represent the viability dose-response of SH-SY5Y cells exposed to (*R*)-(−)-Deprenyl and compounds **12**, **13**, **15**, **16**, **18**, **19** and **20** at 12.5 μM, 25 μM, 50 μM and 100 μM for 24 h. Cell viability was evaluated using MTS assay and normalized to control cells treated with DMSO (0.2 % as final concentration). Bars represent means, and the error bars represent the standard deviation.

at 500 μM for 24 h, reporting that derivatives **16**, **19** and **20** slightly counteract the effects prompted by 6-OHDA displaying an increase of ~10 % cell viability in SH-SY5Y cells; conversely, (*R*)-(−)-Deprenyl, in co-treatment with 6-OHDA, did not exhibit protective effect in terms of cell viability in SH-SY5Y cell line after 24 h (Fig. 4).

2.3. Molecular modeling

Docking simulation techniques were employed to investigate the benzofuran derivatives molecular recognition with respect to *h*MAOs. Prior to docking calculations, the protonation state of the compounds at pH 7.4 was assessed. For the β-hydroxy benzofuran-3-ol derivatives **1**–**10**, two distinct protonation states were identified: a neutral hydroxyl group, found in less than 1 % of the population, and a deprotonated hydroxyl group, predominant in over 99 % of the population. Thus, the deprotonated state was considered for the computational simulation. Interestingly, the presence of the protonated form under biological conditions cannot be excluded. In this protonated state, an intramolecular hydrogen bond with the adjacent carbonyl group may be established leading to the formation of a stable six-membered ring. This conformational restriction could contribute to the lower activity of the 3-ol derivatives.

Docking results highlighted a better theoretical affinity and thus more productive interactions of the synthetic compounds against *h*MAO-B than *h*MAO-A, although a linear agreement between docking scoring functions and the experimental IC_{50} data was not observed due to the scoring limitation (Tables S1-S2). The complex geometries were visually inspected. In detail, docking simulations revealed that the synthesized compounds were oriented within the *h*MAO-A binding site with the benzofuran ring in the catalytic cleft and the substituted phenyl moiety at the entrance, except for derivatives **1**, **3**, **5** and **9** that showed an inverse orientation. All the derivatives established at least a π-π stacking interaction with Tyr407 and Phe352 in front of the FAD cofactor or with Phe208 at the entrance of the binding site (Table 2). Several steric clashes were observed in the inspected binding pose, especially for the β-hydroxyl benzofuran-3-ol derivatives. These contacts may penalize the *h*MAO-A recognition of the benzofuran derivatives.

The same docking analysis performed on *h*MAO-B showed that some of the benzofuran derivatives oriented in the binding site with the benzofuran ring at the entrance and the substituted phenyl moiety in the catalytic cleft, except for derivatives **1**, **2**, **4**, **6**, **9**, **11**, **13**, **15** and **21** that showed a reversed orientation. Compounds **1**, **4**, **7**, and **9** showed a π-π interaction with Tyr326, whereas **10** showed π-π interactions with Phe343 and Trp119, along with an additional hydrogen bond with Tyr435 (Table 3). *h*MAO-B recognition of **2**, **3**, **5**, **6**, and **8** was only based on weak hydrophobic interaction. **8** represents a noteworthy exception within the series, as it shows measurable inhibitory activity in the micromolar range, unlike other benzofuran-3-ol analogues that share a similar binding orientation. Interestingly, while other inactive compounds such as **1**, **4**, **7**, and **9**, establish π–π stacking interaction with Tyr326, **8** does not show such an interaction in the analysed pose. This is somewhat counterintuitive, given its superior activity. Notably, **8** bears a bromine atom at position 3 of the aromatic ring, while its regioisomer with the bromine at position 4 (**9**) is inactive, as well as other 3- or 4-halogenated derivates (**5**, **6** and **7**). These findings suggest that the relationship between binding mode and activity is not solely dictated by interactions with Tyr326 but may also depend on a combination of electronic and steric factors not properly considered in molecular mechanics-based docking approaches. Compounds **11**–**21** highlighted a π-π stacking with Tyr326 which may be fundamental for the target isoform selectivity. Moreover, fewer steric clashes were observed when compared to the binding mode of the synthesized compound to *h*MAO-A (Fig. 5).

According to experimental inhibition data, theoretical results, in general, showed, for our compounds, a better recognition of *h*MAO-B than *h*MAO-A. Docking suggests that the *h*MAO-A interaction could be penalized by steric hindrance. In fact, the binding pocket of MAO-B is known to be broader than *h*MAO-A [50,51].

*h*MAO-B Ile199 and Tyr326 (replaced by Phe208 and Ile335 in *h*MAO-A, respectively) seem to be key residues for the binding of our compounds. In particular, *h*MAO-B Tyr326 is involved in the molecular recognition of almost all the derivatives. Furthermore, the poor experimentally observed *h*MAOs inhibition of β-hydroxy benzofuran-3-ol derivatives **1**–**10**, may be addressed to their water solvation energy, as these compounds are predicted to basically exist as deprotonated state only (~99 %). Net charge species could energetically prefer to stay in a water environment rather than interact with targets (Table S3).

2.4. In silico pharmacokinetic parameters

With the aim to investigate properties that are fundamental for a proper drug development, we investigated the physical-chemical, pharmacokinetics and medicinal chemistry parameters of the most promising compounds **12**, **13**, **15**, **16**, **18**, **19** and **20** by employing the free web tool SwissADME [52] (Table S5, supporting information). We focused our attention on the parameters influencing the ability of these

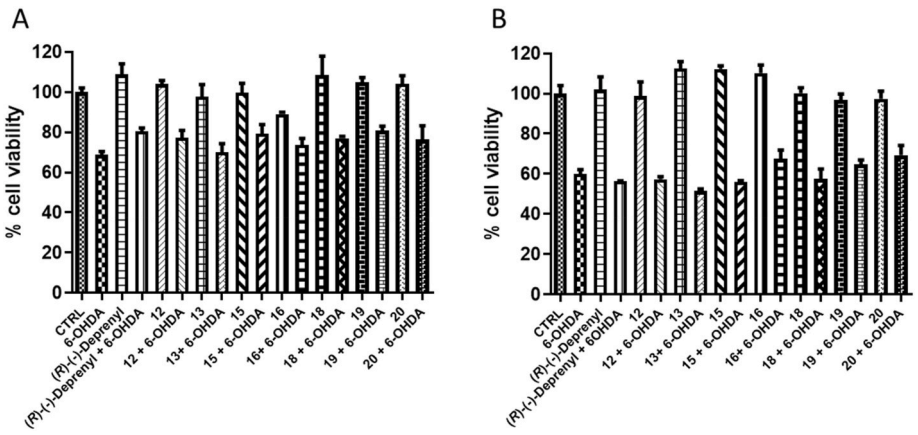

Fig. 4. Cell viability assay. A) Histograms represent the cell viability of SH-SY5Y cells treated with 6-OHDA (500 μM) alone or co-incubated with (*R*)-(−)-Deprenyl, and compounds **12**, **13**, **15**, **16**, **18**, **19,** and **20** at 100 μM for 12 h. B) Histograms represent the cell viability of SH-SY5Y cells treated with 6-OHDA (500 μM) alone or co-incubated with (*R*)-(−)-Deprenyl, and compounds **12**, **13**, **15**, **16**, **18**, **19** and **20** at 100 μM for 24 h. Cell viability was evaluated using MTS assay and normalized to control cells treated with DMSO (0.2 % as final concentration). Bars represent means, and the error bars represent the standard deviation.

Table 2
Docking results of benzofuran derivatives against *h*MAO-A binding site. The most relevant ligand target interaction contribution is reported. HB: hydrogen bond.

Compound	Interactions		
	π-π stacking	HB	Steric clashes
1	–	–	Phe208
2	Tyr407	–	Tyr444/Phe208
3	Tyr407	–	Tyr444/Tyr407
4	Tyr407/Phe208	–	–
5	Tyr407/Phe208	–	Phe208
6	Phe208	–	Asn181/Gln215
7	Tyr407/Phe208	–	–
8	Tyr407	–	Asn181/Tyr444/Tyr407
9	Tyr407	–	Tyr444/P208
10	Tyr407/Phe208	–	Tyr444
11	Tyr407/Phe208	–	–
12	Tyr407/Phe208	–	Tyr444
13	Tyr407/Phe208	–	–
14	Tyr407	–	Tyr407/Leu337
15	Tyr407	–	Tyr407
16	Tyr407	–	Cys323/Tyr407
17	Tyr407/Phe208	–	Tyr407/Tyr444/Leu337
18	Y407/Phe208	–	–
19	P352/Phe208	–	–
20	Tyr407/Phe208	–	Tyr407/Tyr444
21	Tyr407/Phe208/Phe352	–	Tyr407/Tyr444/Cys323

Table 3
Docking results of benzofuran derivatives against *h*MAO-B binding site. The most relevant ligand target interaction contribution is reported.

Compound	Interactions		
	π-π stacking	π-π stacking	π-π stacking
1	Tyr326	–	–
2	–	–	–
3	–	–	–
4	Tyr326	–	–
5	–	–	–
6	–	–	–
7	Tyr326	–	–
8	–	–	–
9	Tyr326	–	–
10	Phe343/Trp119	Tyr435	–
11	Tyr326	–	–
12	Tyr326	–	–
13	Tyr326	–	–
14	Tyr326	–	–
15	Tyr326	–	–
16	Tyr326	–	–
17	Tyr326	–	Tyr435
18	Tyr326	–	–
19	Tyr326	–	–
20	Tyr326	–	–
21	Tyr326/Tyr398	Tyr435	Cys172

derivatives to act as anti-PD drugs by evaluating their drug-likeness and their ability to reach the central nervous system (CNS). The drug-likeness has been evaluated by considering the Lipinski's *rule of five* [53], a method based on experimental and computational approaches employed to approximate solubility and membrane permeability of developing drugs and establishes, in a foreseeable manner, if the target compounds will be effective as oral drugs [54]. This approach has been named *rule of five* because this number (or its multiples) define the threshold of some important properties affecting absorption after oral administration. If there are more than (i) 5 hydrogen-bond donors and (ii) 10 (5 × 2) hydrogen-bond acceptors, (iii) a molecular weight greater than 500 (5 × 100) and (iv) a calculated Log P (cLogP) greater than 5, poor absorption is more likely to take place [54]. Interestingly, all the tested compounds comply with the limits of the Lipinski's rule (Table S5, supporting information). Indeed, all of them possess a number of hydrogen-bond donors and acceptors that are less than 5 and 10, respectively, an average molecular weight of 267.34 with values ranking from 236.27 to 301.13 that are less than the limit of 500, and an estimated cLogP of less than five.

These results are further supported by the estimated gastrointestinal (GI) absorption, i.e. the capability of the compounds to be passively adsorbed in the GI tract after oral administration, that resulted to be high for all the examined compounds, thus additionally sustaining their feasible oral use (Table S5, supporting information).

As stated above, another important attribute that anti-PD drugs should possess, is the aptitude to reach the target enzymes inside the CNS thus overcoming the blood-brain barrier (BBB). The BBB is a physiological protective semipermeable barrier interposed between the CNS and the circulatory system, aimed at preventing xenobiotics access to the brain. This protective role led the BBB to dramatically affect the biodistribution of the drugs in the CNS, being supposed to prevent more than 98 % of small compound drugs and nearly 100 % of large molecule therapeutics from penetrating the brain, thus dramatically affecting their pharmacological efficacy [55,56]. However, compounds endowed with proper characteristics, in particular lipid-solubility, can cross the BBB through a strict selective interface of tight junctions along the basement membrane [57–60]. It is possible to predict the probability

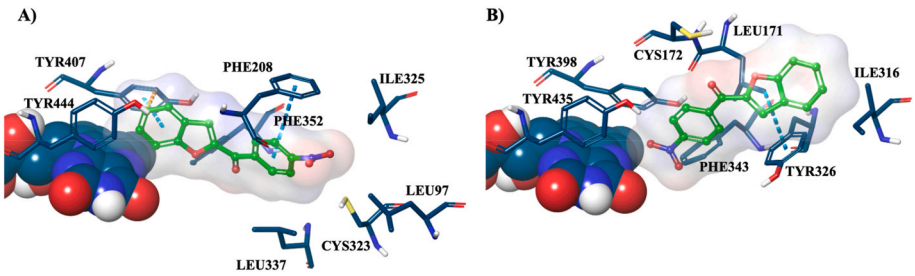

Fig. 5. 3D representation of the best scoring binding poses of **20** in the (**A**) *h*MAO-A and (**B**) *h*MAO-B binding site. The ligands are shown as green sticks, FAD cofactor as blue sphere and amino acids engaged in pivotal contacts with the ligands represented as blue sticks. π−π stacking and bad contacts are represented by azure and orange dashed lines, respectively. (For interpretation of the references to colour in this figure legend, the reader is referred to the Web version of this article.)

that compounds cross the BBB by evaluating two parameters describing lipophilicity (WLOGP) and apparent polarity (TPSA), respectively (Fig. 6) [61]. These two parameters have been employed to set up the Brain Or IntestinaL EstimateD permeation method (BOILED-Egg), a predictive model that works by computing the lipophilicity and polarity of small molecules [61]. The boiled-egg graph allows, at first glance, to simultaneously define two ADME parameters areas, one including the passive absorption through the gastrointestinal tract (white area) and the other considering the ability to permeate the blood brain barrier (BBB, yellow area), along with the susceptibility to P-gp (P-gp) depending on the colour of the dot (Fig. 6). Interestingly, all the examined compounds exhibited the ability to cross the BBB along with a low inclination to be subjected to P-gp activity (Fig. 6). ATP-binding cassette (ABC) transporters, whose P-gp is an example, are critical and selective elements of the BBB. Albeit originally discovered for their capacity to confer multidrug resistance to tumor cells against a range of anticancer agents, P-glycoproteins are emerging as pivotal in limiting the access of drugs to the CNS [62]. Indeed, compounds that are substrates of this protein have a greater chance of being excluded by the CNS. Interestingly, the tested compounds were not predicted to be P-gp substrates, thus further supporting their expected ability to reach the CNS (Table S5, supporting information). Finally, the presence of PAINS

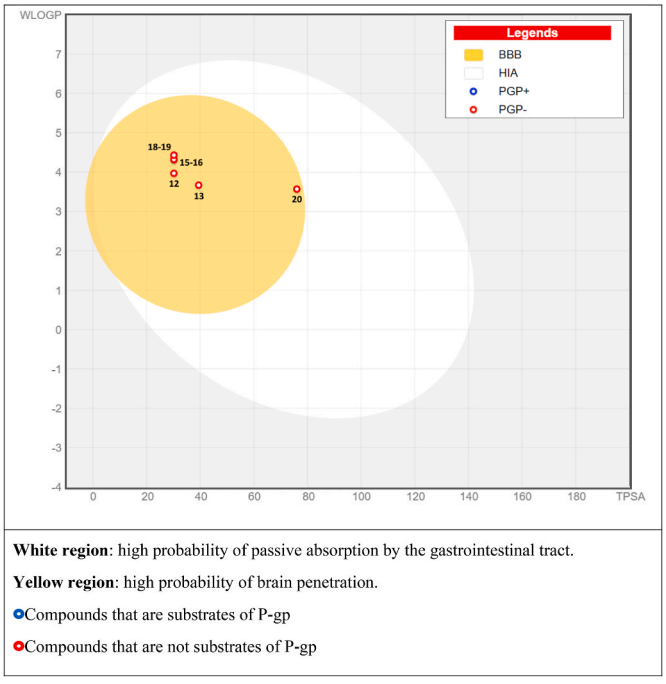

Fig. 6. Representation of the boiled-egg graph calculated by SwissADME web-tool for compounds **12**, **13**, **15**, **16**, **18**, **19** and **20**.

(Pan Assay Interference Compounds), i.e. substructures endowed with the ability to prompt promiscuous pharmacological behaviour, was also evaluated. None of the compounds contain PAINS alerts (Table S5, supporting information).

3. Conclusion

The inhibition of human monoamine oxidase B in the treatment of Parkinson's disease is a well-established clinical practice, and the need for potent therapeutics urges the development of novel compounds that may be potential candidates for the treatment of neurodegenerative diseases. In our work, we developed two series of compounds: 2-aroyl-benzofuran-3-ols (compounds **1**–**10**) and 2-aroyl benzofurans (compounds **11**–**21**) through, respectively, a microwave-assisted reaction and an easy one-step synthesis. Both procedures allowed to obtain the compounds with moderate to good yields. The evaluation of the inhibitory activity of the compounds through a spectrophotometric procedure revealed that the introduction of the hydroxyl group in position 3 of the benzofuran ring (compounds **1**–**10**) leads to a dramatic decrease in both potency and selectivity. The molecular modelling studies offered a possible explanation of this behaviour, as these compounds, at physiological pH, seem to predominantly exist in their deprotonated form (concerning the 3-hydroxyl group). Because of their net charge and, consequently, their high-water solvation energies, compounds **1**–**10** may not favourably interact with the highly lipophilic active sites of the enzymes [50]. On the other hand, compounds **11**–**21** exhibited a remarkably high *h*MAO-B inhibitory activity *in vitro*, with compounds **13** (R = *para*-OCH_3) and **20** (R = *para*-NO_2) showing IC_{50} values of 8.5 and 8.2 nM, respectively. Nonetheless, compounds **12**, **15**, **16**, **18** and **19** were also potent and selective *h*MAO-B inhibitors, presenting IC_{50} values lower than 30 nM. These promising results, as predicted by the performed docking simulation, may derive from the interactions of the 2-aroyl benzofurans within the *h*MAO-B active site, especially with the key residues Ile199 and Tyr326. The cell viability of the most promising compounds (**12**, **13**, **15**, **16**, **18**, **19,** and **20**) was evaluated in two cell lines hGFs and SH-SY5Y cells by the MTS assay. All the compounds, even at the high concentration of 100 μM, did not reduce cell viability after 24h incubation periods. On the other hand, these compounds, only slightly improved cell viability in PD model obtained from SH-SY5Y neuroblastoma cells treatment with the neurotoxic agent 6-OHDA. Notably, the reduction in cell viability was more effectively mitigated after 12 h than after 24 h, with results comparable to those observed with the reference MAO-B inhibitor (*R*)-(−)-Deprenyl. In addition to these results, the *in silico* prediction of the good drug-likeness of compounds **12**, **13**, **15**, **16**, **18**, **19,** and **20** thanks to the free web tool SwissADME support their use as agents able to act on the CNS.

In conclusion, the design of compounds **11**–**21**, starting from the benzo[*b*]thiophen-3-ole scaffold, has led to potent and selective MAO-B inhibitors with promising *in vitro* and *in silico* behaviours, that represent good candidates for the further development of novel treatments against

PD and other neurodegenerative diseases.

4. Experimental protocols

4.1. General

Solvents and reagents were used as supplied without further purification. Microwave-assisted synthesis was performed using an automatic Biotage Initiator™ 2.0 (Uppsala, Sweden), 2.45-GHz high-frequency microwaves, power range 0–300 W. An IR sensor probe strictly controlled the internal vial temperature. ^{1}H and ^{13}C NMR spectra were recorded at 400 and 101 MHz, respectively, on a Bruker spectrometer using $CDCl_3$ and DMSO-d_6 as the solvents at room temperature. The samples were analysed with a final concentration of ~30 mg/mL. Chemical shifts are expressed as δ units (parts per million) relative to the solvent signal. ^{1}H spectra are reported as follows: δ_H (spectrometer frequency, solvent): chemical shift/ppm (multiplicity, *J*-coupling constant(s), number of protons, assignment). ^{13}C spectra are reported as follows: δ_C (spectrometer frequency, solvent): chemical shift/ppm (*J*-coupling constant C–F, assignment). Multiplicity is abbreviated as follows: br – broad; s – singlet; d – doublet; dd – doublet of doublets; ddd – doublet of doublets of doublets; t – triplet; dt – doublets of triplets; q – quartet; m – multiplet. Coupling constants *J* are given in Hertz (Hz). The processing and analyses of the NMR data were carried out with MestreNova. Accurate mass measurements were performed using an Orbitrap Exploris 120 mass spectrometer equipped with an electrospray ionization (ESI) source, featuring the high-flow H-ESI II probe. (Thermo-Fisher Scientific, Waltham, MA, USA). The compounds were dissolved in acetonitrile to a concentration of 10^{-4} M and submitted to automated flow injection analysis (FIA) using the autosampler and pump modules of a Vanquish Core HPLC System (Thermo-Fisher Scientific, Waltham, MA, USA). Briefly, 10 μl of each sample was infused into a continuously flowing stream of acetonitrile, 0.1 % formic acid (V/V) at a flow rate of 0.200 ml/min. Typical source parameters were set as follows: positive ion voltage 3000 V, sheath gas (N_2) 35 arb. unit, auxiliary gas (N_2) 7 arb. unit, ion transfer tube temperature 320 °C, and vaporizer temperature 275 °C.

Mass spectra were acquired in positive ion mode over a mass range of 80–800 Da with a mass resolution of 120000 @ *m/z* 200 and an injection time of 100 ms. Fluorantrene was used as an internal lock mass by activating the EASY-IC source option allowing for a scan-*to*-scan mass scale recalibration in each analysis. The instrument was daily calibrated with Flexmix Calibration solution (Thermo-Fisher Scientific, Waltham, MA, USA). Raw data were processed by using FreeStyle software v. 1.8 provided with the Xcalibur package. Delta values < 1 ppm between theoretical and experimental masses were obtained for all the compounds analysed. Column chromatography was carried out using Sigma-Aldrich® silica gel (high purity grade, pore size 60 Å, 230–400 mesh particle size). All the purifications and reactions were monitored by TLC which was performed on 0.2 mm thick silica gel-aluminium backed plates (60 F_{254}, Merck). Visualization was carried out under ultra-violet irradiation (254 nm). Where given, systematic compound names are those generated by ChemBioDraw Ultra 12.0 following IUPAC conventions. Recombinant MAO-A and MAO-B, expressed in baculovirus infected BTI insect cells, were obtained from Sigma-Aldrich. Kynuramine dihydrobromide (CAS: 304-47-2) was obtained from ChemCruz; *R*-(−)-Deprenyl hydrochloride (CAS: 14611-52-0, ≥98 %), clorgyline hydrochloride (CAS: 17780-75-5, ≥97 %) and 4-quinolinol (CAS: 611-36-9, 98 %) were obtained from Sigma-Aldrich. 96-Wells plates were transparent BRAND plates, pure Grade™, flat bottom (781602) obtained from Brand Gmbh, Wertheim, Germany. The assays were conducted using the plate reader EnSight HH3400 with software Kaleido 2.0, PerkinElmer, Inc. The data obtained were analysed using GraphPad Prism 8 for Windows, version 8.0.2, GraphPad Software, Inc. *In silico* assessment of ADME parameters was performed by using the online free software SwissADME, a web tool that allows to appraise pharmacokinetics, as well as drug-likeness (the probability of being an oral drug) and medicinal chemistry friendliness (PAINS) of small molecules [52].

4.2. Chemistry

4.2.1. Synthesis and characterization data for compounds 1–21

General synthetic procedure A. The synthesis of the 2-aroylbenzofuran-3-ols (**1**–**10**) has been performed following the procedure previously reported by Zhou and colleagues [43]. To a 2-ml microwave tube containing a solution of methyl salicylate (1.0 eq.) in dry acetone (1.5 mL), were added the proper phenacyl bromide (1.1 eq) and potassium phosphate (K_3PO_4, 1.5 eq.). The sealed microwave tube was irradiated at 100 °C for 15 min. At the end, the vial was allowed to cool at room temperature and a dark orange solid was observed inside. The reaction mixture was then filtered and the solid washed using anhydrous acetone. The obtained solid was then dispersed in an aqueous 4 N HCl solution and the dispersion was left stirring for at least 15 min. The dispersion was then filtered and a solid was obtained. The compounds were purified by crystallization or chromatographic method. Concerning crystallization, the proper compound was dissolved in a round-bottom flask in hot diethyl ether or cyclohexane and the solution was allowed to cool at room temperature, to promote the crystallization. After the formation of the crystals, the solution was filtered and the crystals washed using the same solvent used before.

With regard to chromatographic purification approach, silica gel has been employed as stationary phase and elution has been obtained with a 10:1 vol/vol ratio mixture of petroleum ether:ethyl acetate.

General synthetic procedure B. In an oven dried flask containing a stirring solution of methyl salicylaldehyde (1.0 equiv.) in acetonitrile (CH_3CN, 10 mL), was added anhydrous potassium carbonate (1.5 equiv.). The suspension was stirred for 15 min at room temperature; then, the appropriate α-bromoacetophenone (1.0 equiv.) was added and the temperature was raised to 82 °C (reflux). The progression of reaction was monitored by TLC and completion was usually reached in 6–12 h. The reaction was poured into ice-cold water (30 mL) and the system acidified with 2 N HCl, leading to the complete precipitation of the desired compound. The resulting 2-aroyl benzofuran was collected under vacuum filtration and the crude product was purified by column chromatography on silica gel, employing proper mixtures of *n*-hexane: ethyl acetate in a 12:1 vol/vol ratio as mobile phase. This procedure was employed in order to obtain the compounds **11**–**21** in moderate to good yields and with a good level of purity.

4.2.1.1. (3-hydroxybenzofuran-2-yl)(phenyl)methanone (1). Synthesized according to general synthetic procedure A using 2-bromoacetophenone. Yellow powder, yield = 56 %. Chemical Formula: $C_{15}H_{10}O_3$, Molecular Weight: 238,2420 g/mol ^{1}H NMR (400 MHz, $CDCl_3$): δ 7.33 (m, 1H, benzofuran), 7.51 (d, $J = 8.4$ Hz, 1H, benzofuran), 7.57 (m, 3H, Ar), 7.63 (m, 1H, benzofuran), 7.84 (dd, $J = 7.9$, 1.0 Hz, 1H benzofuran), 8.39 (m, 2H, Ar), 11.12 (br s, 1H, OH, D_2O exch.). Experimental in agreement with reported data [43]. Measured monoisotopic mass $[C_{15}H_{10}O_3+H]^+$: *m/z* 239.0703 (Δ: 0.22 ppm) – Theoretical monoisotopic mass: *m/z* 239.07027.

4.2.1.2. (3-hydroxybenzofuran-2-yl)(p-tolyl)methanone (2). Synthesized according to general synthetic procedure A using 2-bromo-1-(*p*-tolyl) ethan-1-one. Yellow powder, yield = 49 %. Chemical Formula: $C_{16}H_{12}O_3$, Molecular Weight: 252,2690 g/mol ^{1}H NMR (400 MHz, DMSO-d_6): δ 2.42 (s, 3H, CH_3), 7.37 (m, 3H, 2H Ar + 1H benzofuran), 7.62 (m, 2H, benzofuran), 7.92 (d, $J = 7.9$ Hz, 1H, benzofuran), 7.9 (d, $J = 8.0$ Hz, 2H, Ar). Experimental in agreement with reported data [43]. Measured monoisotopic mass $[C_{16}H_{12}O_3+H]^+$: *m/z* 253.0860 (Δ: 0.15 ppm) – Theoretical monoisotopic mass: *m/z* 253.08592.

4.2.1.3. (3-hydroxybenzofuran-2-yl)(3-methoxyphenyl)methanone (3). Synthesized according to general synthetic procedure A using 2-bromo-1-(3-methoxyphenyl)ethan-1-one. Yellow powder, yield = 62 %. Chemical Formula: $C_{16}H_{12}O_4$, Molecular Weight: 268,2680. ^{1}H NMR (400 MHz, $CDCl_3$): δ 3.86 (s, 3H, CH_3), 7.18 (m, 1H, Ar), 7.33 (m, 1H, benzofuran), 7.50 (m, 2H, 1H Ar + 1H benzofuran), 7.58 (m, 1H, benzofuran), 7.85 (m, 2H, Ar), 8.05 (dt, J = 7.7, 1.3 Hz, 1H, benzofuran), 11.22 (br s, 1H, OH, D_2O exch.). ^{13}C NMR (101 MHz, DMSO-d_6): δ 55.77 (OCH_3), 113.12 (benzofuran), 114.39 (Ar), 118.67 (Ar), 121.44 (benzofuran), 121.80 (Ar), 122.02 (benzofuran), 123.66 (benzofuran), 130.02 (benzofuran), 130.60 (Ar), 135.66 (benzofuran), 138.86 (Ar), 150.52 (benzofuran), 153.82 (benzofuran), 159.48 (Ar), 182.83 (C═O) Measured monoisotopic mass $[C_{16}H_{12}O_4+H]^+$: *m/z* 269.0809 (Δ: 0.17 ppm) – Theoretical monoisotopic mass: *m/z* 269.08084.

4.2.1.4. (3-hydroxybenzofuran-2-yl)(4-methoxyphenyl)methanone (4). Synthesized according to general synthetic procedure A using 2-bromo-1-(4-methoxyphenyl)ethan-1-one. Yellow powder, yield = 55 %. Chemical Formula: $C_{16}H_{12}O_4$, Molecular Weight: 268,2680. ^{1}H NMR (400 MHz, DMSO-d_6): δ 3.89 (s, 3H, CH_3), 7.13 (m, 2H, Ar), 7.37 (t, J = 7.4 Hz, 1H, benzofuran), 7.63 (m, 2H, benzofuran), 7.90 (d, J = 7.9 Hz, 1H, benzofuran), 8.13 (m, 2H, Ar). Experimental in agreement with reported data [43]. Measured monoisotopic mass $[C_{16}H_{12}O_4+H]^+$: *m/z* 269.0809 (Δ: 0.22 ppm) – Theoretical monoisotopic mass: *m/z* 269.08084.

4.2.1.5. (4-fluorophenyl)(3-hydroxybenzofuran-2-yl)methanone (5). Synthesized according to general synthetic procedure A using 2-bromo-1-(4-fluorophenyl)ethan-1-one. Yellow powder, yield = 61 %. Chemical Formula: $C_{15}H_9FO_3$, Molecular Weight: 256,2324. ^{1}H NMR (400 MHz, $CDCl_3$): δ 7.16 (m, 2H, Ar), 7.23 (m, 1H, benzofuran), 7.41 (m, 1H, benzofuran), 7.50 (t, J = 7.9 Hz, 1H, benzofuran), 7.75 (d, J = 7.7 Hz, 1H, benzofuran), 8.36 (m, 2H, Ar), 10.64 (br s, 1H, OH, D_2O exch.). ^{13}C NMR (101 MHz, DMSO-d_6): δ 113.09 (benzofuran), 115.87 (2 x Ar, $^2J_{C\text{-}F}$ = 21.9 Hz), 121.44 (benzofuran), 122.05 (benzofuran), 123.66 (benzofuran), 130.59 (benzofuran), 132.36 (2 x Ar, $^3J_{C\text{-}F}$ = 9.4 Hz), 134.15 (Ar, $^4J_{C\text{-}F}$ = 2.9 Hz), 135.53 (benzofuran), 150.40 (benzofuran), 153.83 (benzofuran), 165.00 (Ar, $^1J_{C\text{-}F}$ = 250.5 Hz), 181.69 (C═O). Measured monoisotopic mass $[C_{15}H_9FO_3+H]^+$: *m/z* 257.0608 (Δ: 0.11 ppm) – Theoretical monoisotopic mass: *m/z* 257.06085.

4.2.1.6. (3-chlorophenyl)(3-hydroxybenzofuran-2-yl)methanone (6). Synthesized according to general synthetic procedure A using 2-bromo-1-(3-chlorophenyl)ethan-1-one. Yellow powder, yield = 47 %. Chemical Formula: $C_{15}H_9ClO_3$, Molecular Weight: 272,6840. ^{1}H NMR (400 MHz, $CDCl_3$): δ 7.34 (t, J = 7.5 Hz, 1H, benzofuran), 7.51 (m, 2H, 1H Ar + 1H benzofuran), 7.60 (m, 2H, 1H Ar + 1H benzofuran), 7.84 (d, J = 7.9 Hz, 1H, benzofuran), 8.28 (dt, J = 7.7, 1.5 Hz, 1H, Ar), 8.35 (t, J = 1.9 Hz, 1H, Ar), 10.97 (br s, 1H, OH, D_2O exch.). ^{13}C NMR (101 MHz, DMSO-d_6): δ 113.12 (benzofuran), 121.53 (benzofuran), 122.26 (benzofuran), 123.66 (benzofuran), 127.98 (Ar), 128.96 (Ar), 130.75 (benzofuran), 130.78 (Ar), 132.37 (Ar), 133.47 (Ar), 135.45 (benzofuran), 139.76 (Ar), 150.43 (benzofuran), 154.03 (benzofuran), 181.46 (C═O). Measured monoisotopic mass $[C_{15}H_9{}^{35}ClO_3+H]^+$: *m/z* 273.0313 (Δ: 0.07 ppm) – Theoretical monoisotopic mass: *m/z* 273.03130.

4.2.1.7. (4-chlorophenyl)(3-hydroxybenzofuran-2-yl)methanone (7). Synthesized according to general synthetic procedure A using 2-bromo-1-(4-chlorophenyl)ethan-1-one. Yellow powder, yield = 56 %. Chemical Formula: $C_{15}H_9ClO_3$, Molecular Weight: 272,6840. ^{1}H NMR (400 MHz, DMSO-d_6): δ 7.35 (m, 1H, benzofuran), 7.62 (m, 4H, 2H Ar + 2H benzofuran), 7.93 (m, 1H, benzofuran), 8.01 (m, 2H, Ar). Experimental in agreement with reported data [43]. Measured monoisotopic mass $[C_{15}H_9{}^{35}ClO_3+H]^+$: *m/z* 273.0313 (Δ: 0.16 ppm) – Theoretical monoisotopic mass: *m/z* 273.03130.

4.2.1.8. (3-bromophenyl)(3-hydroxybenzofuran-2-yl)methanone (8). Synthesized according to general synthetic procedure A using 2-bromo-1-(3-bromophenyl)ethan-1-one. Yellow powder, yield = 43 %. Chemical Formula: $C_{15}H_9BrO_3$, Molecular Weight: 317,1380. ^{1}H NMR (400 MHz, $CDCl_3$): δ 7.35 (m, 1H, benzofuran), 7.45 (t, J = 7.9 Hz, 1H, Ar), 7.52 (d, J = 8.4 Hz, 1H, benzofuran), 7.60 (m, 1H, benzofuran), 7.75 (m, 1H, Ar), 7.85 (d, J = 7.7 Hz, 1H, benzofuran), 8.33 (dt, J = 7.8, 1.4 Hz, 1H, Ar), 8.49 (t, J = 1.9 Hz, 1H, Ar), 10.97 (s, 1H, OH, D_2O exch.). ^{13}C NMR (101 MHz, DMSO-d_6): δ 113.12 (benzofuran), 121.54 (benzofuran), 121.88 (Ar), 122.28 (benzofuran), 123.66 (benzofuran), 128.35 (Ar), 130.75 (benzofuran), 131.03 (Ar), 131.81 (Ar), 135.25 (Ar), 135.43 (benzofuran), 140.00 (Ar), 150.37 (benzofuran), 154.04 (benzofuran), 181.42 (C═O). Measured monoisotopic mass $[C_{15}H_9{}^{79}BrO_3+H]^+$: *m/z* 316.9808 (Δ: 0.06 ppm) – Theoretical monoisotopic mass: *m/z* 316.98078.

4.2.1.9. (4-bromophenyl)(3-hydroxybenzofuran-2-yl)methanone (9). Synthesized according to general synthetic procedure A using 2-bromo-1-(4-bromophenyl)ethan-1-one. Yellow powder, yield = 52 %. Chemical Formula: $C_{15}H_9BrO_3$, Molecular Weight: 317,1380. ^{1}H NMR (400 MHz, $CDCl_3$): δ 7.21 (m, 1H, benzofuran), 7.25 (m, 1H, Ar), 7.32 (t, J = 7.5 Hz, 1H, benzofuran), 7.49 (d, J = 8.5 Hz, 1H, benzofuran), 7.57 (m, 1H, benzofuran), 7.82 (d, J = 8.0 Hz, 1H, Ar), 8.43 (m, 2H, Ar), 11.02 (br s, 1H, OH, D_2O exch.). Experimental in agreement with reported data [43]. Measured monoisotopic mass $[C_{15}H_9{}^{79}BrO_3+H]^+$: *m/z* 316.9808 (Δ: 0.16 ppm) – Theoretical monoisotopic mass: *m/z* 316.98078.

4.2.1.10. [1,1′-biphenyl]-4-yl(3-hydroxybenzofuran-2-yl)methanone (10). Synthesized according to general synthetic procedure A using 1-([1,1′-biphenyl]-4-yl)-2-bromoethan-1-one. Yellow powder, yield = 45 %. Chemical Formula: $C_{21}H_{14}O_3$, Molecular Weight: 314,3400. ^{1}H NMR (400 MHz, $CDCl_3$): δ 7.34 (t, J = 7.4 Hz, 1H, benzofuran), 7.44 (m, 1H, Ar), 7.51 (m, 3H, 2H Ar + 1H benzofuran), 7.59 (m, 1H, benzofuran), 7.69 (m, 2H, Ar), 7.80 (d, J = 8.2 Hz, 2H, Ar), 7.86 (d, J = 7.9 Hz, 1H, benzofuran), 8.48 (d, J = 8.1 Hz, 2H, Ar), 11.13 (br s, 1H, OH, D_2O exch.). Experimental in agreement with reported data [43]. Measured monoisotopic mass $[C_{21}H_{14}O_3+H]^+$: *m/z* 315.1017 (Δ: 0.26 ppm) – Theoretical monoisotopic mass: *m/z* 315.10157.

4.2.1.11. Benzofuran-2-yl(phenyl)methanone (11). Synthesized according to general synthetic procedure B using 2-bromo-1-phenylethan-1-one. White powder, yield = 46 %. Chemical Formula: $C_{15}H_{10}O_2$, Molecular Weight: 222,2430. ^{1}H NMR (400 MHz, DMSO-d_6): δ 7.36–7.45 (m, 1H, benzofuran), 7.61 (ddd, J = 13.7, 8.2, 6.8 Hz, 3H, 2H Ar + 1H benzofuran), 7.69–7.81 (m, 3H, 1H Ar + 2H benzofuran), 7.88 (dt, J = 7.9, 1.0 Hz, 1H, benzofuran), 7.97–8.04 (m, 2H, Ar). ^{13}C NMR (101 MHz, $CDCl_3$): δ 112.59 (benzofuran), 116.58 (benzofuran), 123.35 (benzofuran), 124.01 (benzofuran), 127.03 (benzofuran), 128.41 (benzofuran), 128.57 (2 x Ar), 129.47 (2 x Ar), 132.93 (Ar), 137.26 (Ar), 152.24 (benzofuran), 156.03 (benzofuran), 184.43 (C═O). Measured monoisotopic mass $[C_{15}H_{10}O_2+H]^+$: *m/z* 223.0754 (Δ: 0.17 ppm) – Theoretical monoisotopic mass: *m/z* 223.07536.

4.2.1.12. Benzofuran-2-yl(p-tolyl)methanone (12). Synthesized according to general synthetic procedure B using 2-bromo-1-(*p*-tolyl)ethan-1-one. White powder, yield = 56 %. Chemical Formula: $C_{16}H_{12}O_2$, Molecular Weight: 236,2700. ^{1}H NMR (400 MHz, DMSO-d_6): δ 2.44 (s, 3H, CH_3), 7.36–7.49 (m, 3H, 2H Ar + 1H benzofuran), 7.56–7.60 (m, 1H, benzofuran), 7.74–7.81 (m, 2H, benzofuran), 7.84–7.90 (m, 1H, benzofuran), 7.90–7.96 (m, 2H, Ar). ^{13}C NMR (101 MHz, $CDCl_3$): δ 21.67 (CH_3), 112.71 (benzofuran), 117.15 (benzofuran), 124.30 (benzofuran), 124.59 (benzofuran), 127.30 (benzofuran), 129.04 (benzofuran), 129.81 (4 x Ar), 134.55 (Ar), 144.16 (Ar), 151.98 (benzofuran), 155.68 (benzofuran), 183.61 (C═O). Measured monoisotopic mass $[C_{16}H_{12}O_2+H]^+$: *m/z* 237.0911 (Δ: 0.25 ppm) – Theoretical monoisotopic mass: *m/z* 237.09101.

4.2.1.13. Benzofuran-2-yl(4-methoxyphenyl)methanone (13). Synthesized according to general synthetic procedure B using 2-bromo-1-(4-methoxyphenyl)ethan-1-one. White powder, yield = 52 %. Chemical Formula: $C_{16}H_{12}O_3$, Molecular Weight: 252,2690. ^{1}H NMR (400 MHz, $CDCl_3$): δ 3.93 (s, 3H, OCH_3), 7.03–7.06 (m, 2H, Ar), 7.35 (t, J = 7.6 Hz, 1H, benzofuran), 7.49–7.55 (m, 2H, benzofuran), 7.66 (d, J = 8.4 Hz, 1H, benzofuran), 7.75 (d, J = 8.0 Hz, 1H, benzofuran), 8.13–7.16 (m, 2H, Ar). ^{13}C NMR (101 MHz, $CDCl_3$): δ 55.57 (OCH_3), 112.51 (benzofuran), 113.87 (2 x Ar), 115.54 (benzofuran), 123.17 (benzofuran), 123.90 (benzofuran), 127.08 (benzofuran), 128.03 (2 x Ar), 129.85 (benzofuran), 132.00 (2 x Ar), 152.71 (benzofuran), 155.84 (benzofuran), 163.63 (Ar), 182.88 (C═O). Measured monoisotopic mass $[C_{16}H_{12}O_3+H]^+$: *m/z* 253.0860 (Δ: 0.32 ppm) – Theoretical monoisotopic mass: *m/z* 253.08592.

4.2.1.14. Benzofuran-2-yl(4-fluorophenyl)methanone (14). Synthesized according to general synthetic procedure B using 2-bromo-1-(4-fluorophenyl)ethan-1-one. White powder, yield = 48 %. Chemical Formula: $C_{15}H_9FO_2$, Molecular Weight: 240,2334. ^{1}H NMR (400 MHz, $CDCl_3$): 7.23 (t, J = 8.4 Hz, 2H, Ar), 7.36 (t, J = 7.5 Hz, 1H, benzofuran), 7.52 (t, J = 7.7 Hz, 1H, benzofuran), 7.57 (s, 1H, benzofuran), 7.65 (d, J = 8.4 Hz, 1H, benzofuran), 7.75 (d, J = 7.9 Hz, 1H, benzofuran), 8.14 (dd, J = 8.4, 5.3 Hz, 2H, Ar). ^{13}C NMR (101 MHz, $CDCl_3$): δ 112.56 (benzofuran), 115.77 (d, $^2J_{CF}$ = 22.0 Hz, 2 x Ar), 116.33 (benzofuran), 123.34 (benzofuran), 124.10 (benzofuran), 126.94 (benzofuran), 128.47 (benzofuran), 132.20 (d, $^3J_{CF}$ = 9.1 Hz, 2 x Ar), 133.39 (d, $^4J_{CF}$ = 3.0 Hz, Ar), 152.21 (benzofuran), 155.99 (benzofuran), 165.70 (d, $^1J_{CF}$ = 254.9 Hz, Ar), 182.70 (C═O). Measured monoisotopic mass $[C_{15}H_9FO_2+H]^+$: *m/z* 241.0660 (Δ: 0.22 ppm) – Theoretical monoisotopic mass: *m/z* 241.06593.

4.2.1.15. Benzofuran-2-yl(3-chlorophenyl)methanone (15). Synthesized according to general synthetic procedure B using 2-bromo-1-(3-clorophenyl)ethan-1-one. White powder, yield = 41 %. Chemical Formula: $C_{15}H_9ClO_2$, Molecular Weight: 256,6850. ^{1}H NMR (400 MHz, $CDCl_3$): δ 7.34–7.38 (m, 1H, benzofuran), 7.48–7.55 (m, 2H, Ar), 7.57 (d, J = 1.1 Hz, 1H, benzofuran), 7.61–7.67 (m, 2H, benzofuran), 7.75–7.77 (m, 1H, Ar), 7.94–7.97 (dt, J = 7.7, 1.4 Hz, 1H, benzofuran), 8.04 (t, J = 1.9 Hz, 1H, Ar). ^{13}C NMR (101 MHz, $CDCl_3$): δ 112.62 (benzofuran), 116.94 (benzofuran), 123.47 (benzofuran), 124.18 (benzofuran), 126.89 (benzofuran), 127.59 (Ar), 128.74 (benzofuran), 129.45 (Ar), 129.92 (Ar), 132.88 (Ar), 134.80 (Ar), 138.70 (Ar), 151.82 (benzofuran), 156.11 (benzofuran), 182.82 (C═O). Measured monoisotopic mass $[C_{15}H_9^{35}ClO_2+H]^+$: *m/z* 257.0365 (Δ: 0.30 ppm) – Theoretical monoisotopic mass: *m/z* 257.03638.

4.2.1.16. Benzofuran-2-yl(4-chlorophenyl)methanone (16). Synthesized according to general synthetic procedure B using 2-bromo-1-(4-clorophenyl)ethan-1-one. White powder, yield = 57 %. Chemical Formula: $C_{15}H_9ClO_2$, Molecular Weight: 256,6850. ^{1}H NMR (400 MHz, $CDCl_3$): δ 7.21–7.29 (m, 1H, benzofuran), 7.39–7.45 (m, 3H, 2H Ar + 1H benzofuran), 7.45–7.48 (m, 1H, benzofuran), 7.55 (d, J = 8.4 Hz, 1H, benzofuran), 7.65 (d, J = 7.8 Hz, 1H, benzofuran), 7.90–7.97 (m, 2H, Ar). ^{13}C NMR (101 MHz, $CDCl_3$): δ 112.58 (benzofuran), 116.51 (benzofuran), 123.39 (benzofuran), 124.13 (benzofuran), 126.92 (benzofuran), 128.58 (benzofuran), 128.91 (2 x Ar), 130.95 (2 x Ar), 135.42 (Ar), 139.45 (Ar), 152.09 (benzofuran), 156.03 (benzofuran), 182.95 (C═O). Measured monoisotopic mass $[C_{15}H_9^{35}ClO_2+H]^+$: *m/z* 257.0364 (Δ: 0.15 ppm) – Theoretical monoisotopic mass: *m/z* 257.03638.

4.2.1.17. Benzofuran-2-yl(2,4-dichlorophenyl)methanone (17). Synthesized according to general synthetic procedure B using 2-bromo-1-(2,4-dichlorophenyl)ethan-1-one. White powder, yield = 39 %. Chemical Formula: $C_{15}H_8Cl_2O_2$, Molecular Weight: 291,1270. ^{1}H NMR (400 MHz, $CDCl_3$): δ 7.23–7.32 (m, 3H, 2H Ar + 1H benzofuran), 7.40–7.45 (m, 3H, 1H Ar + 2H benzofuran), 7.49–7.56 (m, 1H, benzofuran), 7.58–7.65 (m, 1H, benzofuran). ^{13}C NMR (101 MHz, $CDCl_3$): δ 112.72 (benzofuran), 117.71 (benzofuran), 123.63 (benzofuran), 124.26 (benzofuran), 126.93 (benzofuran), 127.11 (benzofuran), 129.17 (Ar), 130.37 (2 x Ar), 132.97 (Ar), 135.74 (Ar), 137.42 (Ar), 151.72 (benzofuran), 156.43 (benzofuran), 182.84 (C═O). Measured monoisotopic mass $[C_{15}H_8^{35}Cl_2O_2+H]^+$: *m/z* 290.9975 (Δ: 0.20 ppm) – Theoretical monoisotopic mass: *m/z* 290.99741.

4.2.1.18. Benzofuran-2-yl(3-bromophenyl)methanone (18). Synthesized according to general synthetic procedure B using 2-bromo-1-(3-bromophenyl)ethan-1-one. White powder, yield = 44 %. Chemical Formula: $C_{15}H_9BrO_2$, Molecular Weight: 301,1390. ^{1}H NMR (400 MHz, $CDCl_3$): δ 7.27 (t, J = 7.5 Hz, 1H, benzofuran), 7.34 (t, J = 7.9 Hz, 1H, Ar), 7.44 (ddd, J = 8.4, 7.1, 1.3 Hz, 1H, benzofuran), 7.48 (d, J = 0.9 Hz, 1H, benzofuran), 7.57 (d, J = 8.4 Hz, 1H, benzofuran), 7.63–7.71 (m, 2H, 1H Ar + 1H benzofuran), 7.91 (dt, J = 7.7, 1.4 Hz, 1H, Ar), 8.10 (t, J = 1.8 Hz, 1H, Ar). ^{13}C NMR (101 MHz, $CDCl_3$): δ 112.64 (benzofuran), 116.97 (benzofuran), 122.79 (Ar), 123.47 (benzofuran), 124.19 (benzofuran), 126.89 (Ar), 128.03 (Ar), 128.75 (benzofuran), 130.16 (benzofuran), 132.34 (Ar), 135.80 (Ar), 138.92 (Ar), 151.79 (benzofuran), 156.12 (benzofuran), 182.74 (C═O). Measured monoisotopic mass $[C_{15}H_9^{79}BrO_2+H]^+$: *m/z* 300.9859 (Δ: 0.21 ppm) – Theoretical monoisotopic mass: *m/z* 300.98587.

4.2.1.19. Benzofuran-2-yl(4-bromophenyl)methanone (19). Synthesized according to general synthetic procedure B using 2-bromo-1-(4-bromophenyl)ethan-1-one. White powder, yield = 53 %. Chemical Formula: $C_{15}H_9BrO_2$, Molecular Weight: 301,1390. ^{1}H NMR (400 MHz, $CDCl_3$): δ 7.26 (t, J = 7.5 Hz, 1H, benzofuran), 7.43 (ddd, J = 8.4, 7.0, 1.3 Hz, 1H, benzofuran), 7.46 (s, 1H, benzofuran), 7.55 (d, J = 8.4 Hz, 1H, benzofuran), 7.57–7.63 (m, 2H, Ar), 7.65 (d, J = 7.9 Hz, 1H, benzofuran), 7.77–7.89 (m, 2H, Ar). ^{13}C NMR (101 MHz, $CDCl_3$): δ 112.59 (benzofuran), 116.56 (benzofuran), 123.40 (benzofuran), 124.15 (benzofuran), 126.91 (benzofuran), 128.12 (Ar), 128.62 (benzofuran), 131.04 (2 x Ar), 131.90 (2 x Ar), 135.84 (Ar), 152.05 (benzofuran), 156.04 (benzofuran), 183.13 (C═O). Measured monoisotopic mass $[C_{15}H_9^{79}BrO_2+H]^+$: *m/z* 300.9860 (Δ: 0.31 ppm) – Theoretical monoisotopic mass: *m/z* 300.98587.

4.2.1.20. Benzofuran-2-yl(4-nitrophenyl)methanone (20). Synthesized according to general synthetic procedure B using 2-bromo-1-(4-nitrophenyl)ethan-1-one. Pale yellow powder, yield = 57 %. Chemical Formula: $C_{15}H_9NO_4$, Molecular Weight: 267,2400. ^{1}H NMR (400 MHz, DMSO-d_6): δ 7.43 (ddd, J = 8.0, 7.1, 0.9 Hz, 1H, benzofuran), 7.62 (ddd, J = 8.5, 7.2, 1.3 Hz, 1H, benzofuran), 7.80 (dt, J = 8.4, 0.9 Hz, 1H, benzofuran), 7.87–7.93 (m, 2H, benzofuran), 8.19–8.26 (m, 2H, Ar), 8.39–8.46 (m, 2H, Ar). ^{13}C NMR (101 MHz, $CDCl_3$): δ 112.85 (benzofuran), 118.85 (benzofuran), 124.26 (2 x Ar), 124.60 (benzofuran), 124.86 (benzofuran), 127.24 (benzofuran), 129.76 benzofuran), 131.00 (2 x Ar) 142.39 (Ar), 150.20 (Ar), 151.37 (benzofuran), 156.02 (benzofuran), 182.81 (C═O). Measured monoisotopic mass $[C_{15}H_9NO_4+H]^+$: *m/z* 268.0604 (Δ: 0.04 ppm) – Theoretical monoisotopic mass: *m/z* 268.06043.

4.2.1.21. [1,1′-biphenyl]-4-yl(benzofuran-2-yl)methanone (21). Synthesized according to general synthetic procedure B using 1-([1,1′-biphenyl]-4-yl)-2-bromoethan-1-one. White powder, yield = 53 %. Chemical Formula: $C_{21}H_{14}O_2$, Molecular Weight: 298,3410. ^{1}H NMR (400 MHz, DMSO-d_6): δ 7.38–7.50 (m, 2H, 1H Ar + 1H benzofuran), 7.50–7.64 (m, 3H, 2H Ar + 1H benzofuran), 7.76–7.83 (m, 3H, 2H Ar + 1H benzofuran), 7.84–7.95 (m, 4H, 2H Ar + 2H benzofuran), 8.09–8.15 (m, 2H, Ar). ^{13}C NMR (101 MHz, $CDCl_3$): δ 112.60 (benzofuran), 116.34 (benzofuran), 123.34 (Ar), 124.03 (benzofuran), 127.06 (benzofuran),

127.23 (2 x Ar), 127.34 (2 x Ar), 128.32 (benzofuran), 128.38 (benzofuran), 129.03 (2 x Ar), 130.16 (2 x Ar), 135.90 (Ar), 139.90 (Ar), 145.76 (Ar), 152.44 (benzofuran), 156.02 (benzofuran), 183.893 (C═O). Measured monoisotopic mass $[C_{21}H_{14}O_2+H]^+$: *m/z* 299.1067 (Δ: 0.26 ppm) – Theoretical monoisotopic mass: *m/z* 299.10666.

4.2.2. Enzymatic inhibition assay procedure

The assay for the evaluation of the inhibitory activity of the compounds is based on the measurement of the conversion rate of a MAO-substrate, kynuramine, into its oxidized metabolite, 4-quinolinol (4-HQ), which absorbs at 316 nm [45]. First, a calibration curve was created using 4-quinolinol solutions at different concentrations (ranging from 0.01 nM to 10 mM). Then, the kinetic properties (specific activity, Michaelis-Menten constant K_M, and maximum speed V_{max}) of the two isoforms were evaluated using solutions with different enzyme concentrations (12.0 mg/mL to 1 mg/mL for MAO-A; 18.0 mg/mL to 1.5 mg/mL for MAO-B) for the measurement of the specific activity, and kynuramine solutions with at least eight different concentration levels (10 μM–200 μM, referred to the concentration in the wells) for the measurement of K_M and V_{max}. The data were evaluated and the kinetic properties found are here reported: for MAO-A K_M = 28,18 μM and V_{max} = 58,88 pmol/min, for MAO-B K_M = 28,58 μM and V_{max} = 47,32 pmol/min. After having fully characterized the enzymes, the inhibitory activity of the compounds was measured. Compound solutions were pipetted in a 96-wells plate, together with kynuramine solution (concentration = 2 x K_M in the well), phosphate buffer (pH = 7.4, NaH_2PO_4 25 mM and Na_2HPO_4 25 mM, pH adjusted using NaOH), and the plate was then incubated at 37 °C for 10 min. Absorbance of the wells was measured every minute, and the last reading (t = 10 min) was used as blank. Then, the enzyme was added (the amount of enzyme added depended on the specific activity, in order to obtain V_{max} = 50 pmol/-min), and the plate was incubated at 37 °C for 30 min, with the absorbance of the wells being measured every minute. The formation of 4-quinolinol was analysed, and the product formation rate, or initial velocity V_0, was obtained from the slope of the (4-HQ) = f(t) curves. Inhibition percentages at 10 μM were obtained from the comparison between the initial velocity of the control well (no inhibitor) and the initial velocity in the presence of the inhibitor. A preliminary screening was performed with all compounds at 10 μM. For those which presented percentages of *h*MAO inhibition ≥50 % (resulting in IC_{50} < 10 μM), the *h*MAOs IC_{50} values were determined. Different concentrations for each inhibitor were tested and analysed as previously described. Dose-response curves were created using the percentage of inhibition as a function of the logarithm of the concentration of the inhibitor. The IC_{50} values were extrapolated from dose−response curves and expressed as means ± standard deviation. IC_{50} values were determined from at least three independent experiments, each performed in triplicate.

The inhibition mechanisms of compounds **13** and **20** against *h*MAO-B were investigated as follow. DMSO solutions of the two inhibitors at concentrations equal to their respective IC_{50} were obtained. Inhibitors solutions were pipetted in a 96-wels plate, together with phosphate buffer and kynuramine solution. The inhibitors were tested using substrate solutions at different concentrations, ranging from 5 to 1000 μM (concentration in the plate well). Absorbance of the wells was measured every minute and the last read (t = 10 min) was used as blank. Then, the enzyme was added (as described in the IC_{50} assay procedure) and the plate was incubated at 37 °C for 1h, absorbance of the wells was measured every minute. The inverse of the slopes of the obtained absorbance curves were plotted against the inverse of the substrate concentrations and Lineweaver-Burk plots were obtained for both compounds and compared with the curve obtained with the substrate without the inhibitor.

4.2.3. Molecular modelling

The synthetic compounds were manually designed using Maestro, and they were properly prepared with the LigPrep tool [63,64]. The protonation states were assessed at pH 7.4 using Epik and OPLS_2005 as force field [65,66]. MarvinSketch was used to check the protonation states of the synthetic compounds at pH 7.4.

Crystallographic structures from the Protein Data Bank (PDB) with IDs 2Z5X and 6FW0 were used as receptor models for MAO-A and MAO-B, respectively [51,67–69]. These PDB structures were optimized using the Protein Preparation Wizard tool [70] which involved fixing missing atoms and FAD bond order, adding hydrogen atoms, and removing co-crystallized water molecules and ligands. For both target theoretical models, the binding site was mimicked by means of a regular box of approximately 64,000 $Å^3$ centered on the FAD N5 atom. Co-crystallized PDB ligands, harmine for MAO-A and chlorophenyl-chromone-carboxamide for MAO-B, were removed.

Docking analysis was performed using the hybrid QM/MM-based quantum polarized ligand docking (QPLD) method as implemented in Glide software [71,72]. Quantum mechanics (QM) and molecular mechanics (MM) approaches were applied to ligand and target atoms, respectively. MM energy contributions were computed considering the OPLS_2005 force field parameters. The Glide SP (standard precision) scoring function estimated preliminary ligand poses for MAOs. Subsequently, density functional theory (DFT) single point energy calculations using the LACVP* basis set and the B3LYP level of theory, was applied for describing ligands charge distribution. Finally, the synthetized compounds with new partial charges, were re-docked into the MAO enzymes. Prime/MM-GBSA was employed to estimate the theoretical binding free energy (ΔG_{bind}) of set of ligands with respect to MAOs, using the default parameters of the Prime software [73].

The Boltzman population weighted average solvation energy of each compound was computed considering conformers randomly generated by 1000 steps of Monte Carlo (MC) search [74]. The OPLS-2005 force field and GB/SA water implicit solvation model were applied to MC generated structures for estimating internal energy.

4.3. Biology

4.3.1. Cell culture

The cell line human gingival fibroblasts (hGFs) were purchased by ATCC (PCS-201-018 ATCC, Manassas, VA, USA) and cultured with Fibroblast Basal Medium (485 mL; ATCC PCS-201-030) added with growth kit (ATCC PCS-201-041) [14,75]. The human neuroblastoma cell line (SH-SY5Y) was purchased by ATCC (ATCC® No. CRL-2266) and cultured with Dulbecco's Modification of Eagle's Medium with 1 g/L glucose, L-glutamine, sodium pyruvate and 10 % of Fetal Bovin Serum. Both cell lines were maintained in an incubator at 37 °C with 5 % CO_2 and 95 % air. When cells reached 75–80 % confluence were split to obtain subcultures.

4.3.2. Cell metabolic activity

The cell metabolic activity of hGF and SH-SY5Y cells was evaluated by the MTS assay (CellTiter 96® Aqueous One Solution Cell Proliferation Assay, Promega, Madison, WI, USA). Specifically, 2.4 × 10^3 hGF/well and 5 × 10^4 SH-SY5Y/well were seeded in a 96-multiwell plate and maintained in culture medium in an incubator for 24 h. Then hGF and SH-SY5Y cells were treated with compounds **12**, **13**, **15**, **16**, **18**, **19**, **20,** and (*R*)-(−)-Deprenyl at 12.5 μM, 25 μM, 50 μM, and 100 μM for 24 h. After 24 h, 20 μL of MTS staining solution was added to each well, and the plates were incubated for 3 h at 37 °C. The absorbance, directly related to cell metabolic activity, was measured for each well using the Synergy™ HT Multi-detection microplate reader (Biotech, Winooski, VT, USA) at a wavelength of 490 nm [76–78]. The same protocol was used to measure the cell viability of SH-SY5Y treated with 6-OHDA at 500 μM as single treatment or in co-treatment with compounds **12**, **13**, **15**, **16**, **18**, **19**, **20**, (*R*)-(−)- Deprenyl at 100 μM for 12 h and 24 h, respectively.

4.3.3. Statistical analysis

Statistical significance was established with GraphPad 5.01 (GraphPad, San Diego, CA, USA) software utilizing one-way ANOVA followed by post hoc Tukey's multiple comparisons analysis. Values of $p < 0.05$ were considered statistically significant.

CRediT authorship contribution statement

Paolo Guglielmi: Writing – review & editing, Writing – original draft, Supervision, Project administration, Investigation, Funding acquisition, Formal analysis, Conceptualization. **Michele Coluccia:** Writing – review & editing, Writing – original draft, Investigation, Formal analysis, Data curation. **Guya Diletta Marconi:** Writing – review & editing, Writing – original draft, Investigation, Formal analysis, Data curation, Conceptualization. **Francesco Ortuso:** Writing – review & editing, Writing – original draft, Software, Investigation, Formal analysis, Data curation. **Francesca Procopio:** Writing – review & editing, Writing – original draft, Methodology, Investigation, Formal analysis, Data curation. **Simone Carradori:** Writing – review & editing, Writing – original draft. **Jacopo Pizzicannella:** Writing – original draft, Formal analysis. **Francesca Arrighi:** Methodology, Investigation, Formal analysis. **Anna Troiani:** Writing – review & editing, Formal analysis, Data curation. **Chiara Salvitti:** Writing – review & editing, Formal analysis, Data curation. **Fernanda Borges:** Writing – review & editing, Writing – original draft, Supervision, Data curation. **Daniel Chavarria:** Writing – review & editing, Writing – original draft, Investigation, Formal analysis, Data curation. **Paola Chimenti:** Writing – review & editing, Writing – original draft, Supervision. **Daniela Secci:** Writing – review & editing, Writing – original draft, Supervision. **Francesca Diomede:** Writing – review & editing, Writing – original draft, Supervision, Funding acquisition, Formal analysis, Data curation, Conceptualization.

Funding

This research was funded by the European Union—Next Generation EU — 2022HXMY4P—CUP D53D23010340006 Research Project By Relevant National Interest (PRIN 2022), Unity is strength: a novel tool based on human MonoAmine Oxidase B Inhibitors and MEsenchymal Stem Cells Secretome. Novel insights into the molecular Ular mechanisms of ParkiNson's (Maobi-Mescs-Union).

This work was also funded by FEDER funds through national funds by FCT – Foundation for Science and Technology under research grants UIDB/00081/2020 (https://doi.org/10.54499/UIDB/00081/2020, CIQUP) UIDP/00081/2020 (https://doi.org/10.54499/UIDP/00081/2020) (CIQUP), and LA/P/0056/2020 (https://doi.org/10.54499/LA/P/0056/2020, IMS).

Declaration of competing interest

The authors declare that they have no known competing financial interests or personal relationships that could have appeared to influence the work reported in this paper.

Acknowledgements

A special thanks to Dr. Luigia Fonticoli for performing the MTS assay.

Appendix A. Supplementary data

Supplementary data to this article can be found online at https://doi.org/10.1016/j.ejmech.2025.117983.

Data availability

Data will be made available on request.

References

[1] R. Vinay, N. Biller-Andorno, A critical analysis of national dementia care guidances, Health Policy 130 (2023), https://doi.org/10.1016/j.healthpol.2023.104736.
[2] B.Y. Turer, N. Sanlier, Relationship of curcumin with aging and alzheimer and parkinson disease, the Most prevalent age-related neurodegenerative diseases: a narrative review, Nutr. Rev. (2024), https://doi.org/10.1093/nutrit/nuae079.
[3] N. Chowdhary, C. Barbui, K.J. Anstey, M. Kivipelto, M. Barbera, R. Peters, L. Zheng, J. Kulmala, R. Stephen, C.P. Ferri, Y. Joanette, H. Wang, A. Comas-Herrera, C. Alessi, K. Suharya, K.J. Mwangi, R.C. Petersen, A.A. Motala, S. Mendis, D. Prabhakaran, A. Bibi Mia Sorefan, A. Dias, R. Gouider, S. Shahar, K. Ashby-Mitchell, M. Prince, T. Dua, Reducing the risk of cognitive decline and dementia: WHO recommendations, Front. Neurol. 12 (2022), https://doi.org/10.3389/fneur.2021.765584.
[4] B.E. Aksoz, E. Aksoz, Vital role of monoamine oxidases and cholinesterases in central nervous System drug research: a sharp dissection of the pathophysiology, comb chem high throughput, Screen 23 (2020) 877–886, https://doi.org/10.2174/1386207323666200220115154.
[5] Y. Huang, L. Mucke, Alzheimer mechanisms and therapeutic strategies, Cell 148 (2012) 1204–1222, https://doi.org/10.1016/j.cell.2012.02.040.
[6] P. Rana, E.F. Franco, Y. Rao, K. Syed, D. Barh, V. Azevedo, R.T.J. Ramos, P. Ghosh, Evaluation of the common molecular basis in alzheimer's and parkinson's diseases, Int. J. Mol. Sci. 20 (2019), https://doi.org/10.3390/ijms20153730.
[7] D.N. Jones, M.A. Raghanti, The role of monoamine oxidase enzymes in the pathophysiology of neurological disorders, J. Chem. Neuroanat. 114 (2021), https://doi.org/10.1016/j.jchemneu.2021.101957.
[8] Z. Özdemir, M.A. Alagöz, Ö.F. Bahçecioğlu, S. Gök, Monoamine Oxidase-B (MAO-B) inhibitors in the treatment of alzheimer's and Parkinson's disease, Curr. Med. Chem. 28 (2021) 6045–6065, https://doi.org/10.2174/0929867328666210203204710.
[9] C. Edmondson, E. Dale, Binda, Monoamine oxidases, in: E.J. Harris, J. Robin, Boekema (Eds.), Membrane Protein Complexes: Structure and Function, Springer Singapore, Singapore, 2018, pp. 117–139, https://doi.org/10.1007/978-981-10-7757-9_5.
[10] L.G. Iacovino, F. Magnani, C. Binda, The structure of monoamine oxidases: past, present, and future, J. Neural Transm. 125 (2018) 1567–1579, https://doi.org/10.1007/s00702-018-1915-z.
[11] H. Gaweska, P.F. Fitzpatrick, Structures and mechanism of the monoamine oxidase family, Biomol. Concepts 2 (2011) 365–377, https://doi.org/10.1515/BMC.2011.030.
[12] R.R. Ramsay, A. Albreht, Kinetics, mechanism, and inhibition of monoamine oxidase, J. Neural Transm. 125 (2018) 1659–1683, https://doi.org/10.1007/s00702-018-1861-9.
[13] K.F. Tipton, 90 years of monoamine oxidase: some progress and some confusion, J. Neural Transm. 125 (2018) 1519–1551, https://doi.org/10.1007/s00702-018-1881-5.
[14] C. Banerjee, D. Tripathy, D. Kumar, J. Chakraborty, Monoamine oxidase and neurodegeneration: mechanisms, inhibitors and natural compounds for therapeutic intervention, Neurochem. Int. 179 (2024), https://doi.org/10.1016/j.neuint.2024.105831.
[15] Y. Santin, J. Resta, A. Parini, J. Mialet-Perez, Monoamine oxidases in age-associated diseases: new perspectives for old enzymes, Ageing Res. Rev. 66 (2021), https://doi.org/10.1016/j.arr.2021.101256.
[16] C. Sanfilippo, P. Castrogiovanni, R. Imbesi, G. Lazzarino, V. Di Pietro, G. Li Volti, D. Tibullo, I. Barbagallo, G. Lazzarino, R. Avola, G. Musumeci, F. Fazio, M. Vinciguerra, M. Di Rosa, Sex-dependent monoamine oxidase isoforms expression patterns during human brain ageing, Mech. Ageing Dev. 197 (2021), https://doi.org/10.1016/j.mad.2021.111516.
[17] I.A. Volchegorskii, S.E. Shemyakov, V.V. Turygin, N.V. Malinovskaya, The age dynamics of monoamine oxidase activity and levels of lipid peroxidation products in the human brain, Neurosci. Behav. Physiol. 34 (2004) 303–305, https://doi.org/10.1023/B:NEAB.0000018736.84877.4f.
[18] M. Naoi, W. Maruyama, K. Inaba-Hasegawa, Type A and B monoamine oxidase in age-related neurodegenerative disorders: their distinct roles in neuronal death and survival, Curr. Top. Med. Chem. 12 (2012) 2177–2188, https://doi.org/10.2174/156802612805219950.
[19] G. Alper, F.K. Girgin, M. Ozgonul, G. Mentes, B. Ersoz, MAO inhibitors and oxidant stress in aging brain tissue, Eur. Neuropsychopharmacol. 9 (1999) 247–252, https://doi.org/10.1016/s0924-977x(98)00035-2.
[20] T. Nagatsu, M. Sawada, Molecular Mechanism of the Relation of Monoamine Oxidase B and its Inhibitors to Parkinson's Disease: Possible Implications of Glial Cells, Springer-Verlag, 2006.
[21] J. Meiser, D. Weindl, K. Hiller, Complexity of dopamine metabolism. http://www.biosignaling.com/content/11/1/34, 2013.
[22] S.A. Marchitti, R.A. Deitrich, V. Vasiliou, Neurotoxicity and metabolism of the catecholamine-derived 3,4-dihydroxyphenylacetaldehyde and 3,4-dihydroxyphenylglycolaldehyde: the role of aldehyde dehydrogenase, Pharmacol. Rev. 59 (2007) 125–150, https://doi.org/10.1124/pr.59.2.1.
[23] P. Sivakumar, K.B. Nagashanmugam, S. Priyatharshni, R. Lavanya, N. Prabhu, S. Ponnusamy, Review on the interactions between dopamine metabolites and α-Synuclein in causing Parkinson's disease, Neurochem. Int. 162 (2023), https://doi.org/10.1016/j.neuint.2022.105461.
[24] Y. Nakamura, S. Arawaka, H. Sato, A. Sasaki, T. Shigekiyo, K. Takahata, H. Tsunekawa, T. Kato, Monoamine oxidase-B inhibition facilitates α-synuclein secretion in vitro and delays its aggregation in rAAV-based rat models of

Parkinson's disease, J. Neurosci. 41 (2021) 7479–7491, https://doi.org/10.1523/JNEUROSCI.0476-21.2021.
[25] D.S. Goldstein, The catecholaldehyde hypothesis: where MAO fits, J. Neural Transm. 127 (2020) 169–177, https://doi.org/10.1007/s00702-019-02106-9.
[26] Z. Qin, D. Hu, S. Han, S.H. Reaney, D.A. Di Monte, A.L. Fink, Effect of 4-hydroxy-2-nonenal modification on α-synuclein aggregation, J. Biol. Chem. 282 (2007) 5862–5870, https://doi.org/10.1074/jbc.M608126200.
[27] M. Csala, T. Kardon, B. Legeza, B. Lizák, J. Mandl, É. Margittai, F. Puskás, P. Száraz, P. Szelényi, G. Bánhegyi, On the role of 4-hydroxynonenal in health and disease, Biochim. Biophys. Acta Mol. Basis Dis. 1852 (2015) 826–838, https://doi.org/10.1016/j.bbadis.2015.01.015.
[28] L. Shi, C. Huang, Q. Luo, E. Rogers, Y. Xia, W. Liu, W. Ma, W. Zeng, L. Gong, J. Fang, L. Tang, A. Cheng, R. Shi, Z. Chen, The association of iron and the pathologies of Parkinson's diseases in MPTP/MPP+-induced neuronal degeneration in non-human primates and in cell culture, Front. Aging Neurosci. 11 (2019), https://doi.org/10.3389/fnagi.2019.00215.
[29] J.F.G. Neuhaus, O.R. Baris, S. Hess, N. Moser, H. Schröder, S.J. Chinta, J. K. Andersen, P. Kloppenburg, R.J. Wiesner, Catecholamine metabolism drives generation of mitochondrial DNA deletions in dopaminergic neurons, Brain 137 (2014) 354–365, https://doi.org/10.1093/brain/awt291.
[30] A. Siddiqui, I. Hanson, J.K. Andersen, Mao-B elevation decreases parkin's ability to efficiently clear damaged mitochondria: protective effects of rapamycin, Free Radic. Res. 46 (2012) 1011–1018, https://doi.org/10.3109/10715762.2012.662277.
[31] B. Mathew, S. Carradori, P. Guglielmi, MdS. Uddin, H. Kim, New aspects of monoamine oxidase B inhibitors: the key role of halogens to open the golden door, Curr. Med. Chem. 28 (2020) 266–283, https://doi.org/10.2174/0929867327666200121165931.
[32] P. Guglielmi, S. Carradori, A. Ammazzalorso, D. Secci, Novel approaches to the discovery of selective human monoamine oxidase-B inhibitors: is there room for improvement? Expet Opin. Drug Discov. 14 (2019) 995–1035, https://doi.org/10.1080/17460441.2019.1637415.
[33] C.D. Monte, M. D'Ascenzio, P. Guglielmi, V. Mancini, S. Carradori, Opening new scenarios for human MAO inhibitors, Cent. Nerv. Syst. Agents Med. Chem. 16 (2016) 98–104, https://doi.org/10.2174/1871524915666150831141705.
[34] W.H. Jost, A critical appraisal of MAO-B inhibitors in the treatment of Parkinson's disease, J. Neural Transm. 129 (2022) 723–736, https://doi.org/10.1007/s00702-022-02465-w.
[35] Y.Y. Tan, P. Jenner, S. Di Chen, Monoamine Oxidase-B inhibitors for the treatment of parkinson's disease: past, present, and future, J. Parkinsons Dis. 12 (2022) 477–493, https://doi.org/10.3233/JPD-212976.
[36] T. Tsuboi, Y. Satake, K. Hiraga, K. Yokoi, M. Hattori, M. Suzuki, K. Hara, A. Ramirez-Zamora, M.S. Okun, M. Katsuno, Effects of MAO-B inhibitors on non-motor symptoms and quality of life in Parkinson's disease: a systematic review, npj Parkinson's Dis. 8 (2022), https://doi.org/10.1038/s41531-022-00339-2.
[37] J.P.M. Finberg, K. Gillman, Selective inhibitors of monoamine oxidase type B and the "cheese effect,", in: Int Rev Neurobiol, Academic Press Inc., 2011, pp. 169–190, https://doi.org/10.1016/B978-0-12-386467-3.00009-1.
[38] P. Guglielmi, D. Secci, A. Petzer, D. Bagetta, P. Chimenti, G. Rotondi, C. Ferrante, L. Recinella, S. Leone, S. Alcaro, G. Zengin, J.P. Petzer, F. Ortuso, S. Carradori, Benzo[b]tiophen-3-ol derivatives as effective inhibitors of human monoamine oxidase: design, synthesis, and biological activity, J. Enzym. Inhib. Med. Chem. 34 (2019) 1511–1525, https://doi.org/10.1080/14756366.2019.1653864.
[39] F. Mesiti, A. Gaspar, D. Chavarria, A. Maruca, R. Rocca, E. Gil Martins, S. Barreiro, R. Silva, C. Fernandes, S. Gul, O. Keminer, S. Alcaro, F. Borges, Mapping Chromone-3-Phenylcarboxamide pharmacophore: quid est veritas? J. Med. Chem. 64 (2021) 11169–11182, https://doi.org/10.1021/acs.jmedchem.1c00510.
[40] J. Reis, C. Fernandes, H. Salem, M. Maia, C. Tomé, S. Benfeito, J. Teixeira, P. J. Oliveira, E. Uriarte, F. Ortuso, S. Alcaro, D. Bagetta, F. Cagide, F. Borges, Design and synthesis of chromone-based monoamine oxidase B inhibitors with improved drug-like properties, Eur. J. Med. Chem. 239 (2022), https://doi.org/10.1016/j.ejmech.2022.114507.
[41] P. Guglielmi, B. Mathew, D. Secci, S. Carradori, Chalcones: unearthing their therapeutic possibility as monoamine oxidase B inhibitors, Eur. J. Med. Chem. 205 (2020), https://doi.org/10.1016/j.ejmech.2020.112650.
[42] E. Mateev, M. Georgieva, A. Mateeva, A. Zlatkov, S. Ahmad, K. Raza, V. Azevedo, D. Barh, Structure-Based design of novel MAO-B inhibitors: a review, Molecules 28 (2023), https://doi.org/10.3390/molecules28124814.
[43] Z.Z. Zhou, Y.H. Deng, Z.H. Jiang, W.H. Chen, Microwave-assisted Dieckmann reaction: efficient one-step synthesis of 2-aroylbenzofuran-3-ols, Adv. Synth. Catal. 352 (2010) 1909–1913, https://doi.org/10.1002/adsc.201000256.
[44] I. Ali, R. Rafique, K.M. Khan, S. Chigurupati, X. Ji, A. Wadood, A.U. Rehman, U. Salar, M.S. Iqbal, M. Taha, S. Perveen, B. Ali, Potent α-amylase inhibitors and radical (DPPH and ABTS) scavengers based on benzofuran-2-yl(phenyl)methanone derivatives: syntheses, in vitro, kinetics, and in silico studies, Bioorg. Chem. 104 (2020), https://doi.org/10.1016/j.bioorg.2020.104238.
[45] S. Giovannuzzi, D. Chavarria, G. Provensi, M. Leri, M. Bucciantini, S. Carradori, A. Bonardi, P. Gratteri, F. Borges, A. Nocentini, C.T. Supuran, Dual inhibitors of brain carbonic anhydrases and monoamine Oxidase-B efficiently protect against Amyloid-β-Induced neuronal toxicity, oxidative stress, and mitochondrial dysfunction, J. Med. Chem. 67 (2024) 4170–4193, https://doi.org/10.1021/acs.jmedchem.4c00045.
[46] M.J. Matos, P. Novo, L. Mayán, I. Torres, E. Uriarte, M. Yáñez, J.Á. Fontenla, F. Ortuso, S. Alcaro, F. Procopio, M.I. Rodríguez-Franco, C. Val, M.I. Loza, J. Brea, F. Borges, D. Viña, 8-Amide and 8-carbamate substitution patterns as modulators of 7-hydroxy-4-methylcoumarin's antidepressant profile: synthesis, biological evaluation and docking studies, Eur. J. Med. Chem. 248 (2023), https://doi.org/10.1016/j.ejmech.2023.115091.
[47] H. Kalasz, K. Magyar, E. Szoke, E. Adeghate, A. Adem, M.Y. Hasan, S.M. Nurulain, K. Takes, Metabolism of selegiline [(-)-Deprenyl)], Curr. Med. Chem. 21 (2014) 1522–1530, https://doi.org/10.2174/09298673216613121809435 2.
[48] D. Hernandez-Baltazar, L.M. Zavala-Flores, A. Villanueva-Olivo, The 6-hydroxydopamine model and parkinsonian pathophysiology: novel findings in an older model. www.elsevier.es/neurologia, 2017.
[49] N. Simola, M. Morelli, A.R. Carta, The 6-Hydroxydopamine model of parkinson's disease, Neurotox. Res. 11 (2007) 151–167, https://doi.org/10.1007/BF03033565.
[50] C. Binda, F. Hubálek, M. Li, D.E. Edmondson, A. Mattevi, Crystal structure of human monoamine oxidase B, a drug target enzyme monotopically inserted into the mitochondrial outer membrane, FEBS Lett. (2004) 225–228, https://doi.org/10.1016/S0014-5793(04)00209-1.
[51] S.-Y. Son, J. Ma, Y. Kondou, M. Yoshimura, E. Yamashita, T. Tsukihara, Structure of human monoamine oxidase A at 2.2-Å resolution: the control of opening the entry for substrates/inhibitors, Proc. Natl. Acad. Sci. 105 (2008) 5739–5744, https://doi.org/10.1073/pnas.0710626105.
[52] A. Daina, O. Michielin, V. Zoete, SwissADME: a free web tool to evaluate pharmacokinetics, drug-likeness and medicinal chemistry friendliness of small molecules, Sci. Rep. 7 (2017), https://doi.org/10.1038/srep42717.
[53] C.A. Lipinski, F. Lombardo, B.W. Dominy, P.J. Feeney, Experimental and computational approaches to estimate solubility and permeability in drug discovery and development q settings. www.elsevier.com/locate/drugdeliv, 2001.
[54] R. Roskoski, Properties of FDA-approved small molecule protein kinase inhibitors: a 2024 update, Pharmacol. Res. 200 (2024), https://doi.org/10.1016/j.phrs.2024.107059.
[55] J.H. Pedder, A.M. Sonabend, M.D. Cearns, B.D. Michael, R. Zakaria, A. B. Heimberger, M.D. Jenkinson, D. Dickens, Crossing the blood-brain barrier: emerging therapeutic strategies for neurological disease, Lancet Neurol. (2025), https://doi.org/10.1016/S1474-4422(24)00476-9.
[56] R. Daneman, A. Prat, The blood–brain barrier, Cold Spring Harbor Perspect. Biol. 7 (2015), https://doi.org/10.1101/cshperspect.a020412.
[57] H. Kadry, B. Noorani, L. Cucullo, A blood–brain barrier overview on structure, function, impairment, and biomarkers of integrity, Fluids Barriers CNS 17 (2020), https://doi.org/10.1186/s12987-020-00230-3.
[58] E.G. Knox, M.R. Aburto, G. Clarke, J.F. Cryan, C.M. O'Driscoll, The blood-brain barrier in aging and neurodegeneration, Mol. Psychiatr. 27 (2022) 2659–2673, https://doi.org/10.1038/s41380-022-01511-z.
[59] G. Schiera, C.M. Di Liegro, G. Schirò, G. Sorbello, I. Di Liegro, Involvement of astrocytes in the Formation, maintenance, and function of the blood–brain barrier, Cells 13 (2024), https://doi.org/10.3390/cells13020150.
[60] F. Pisani, V. Castagnola, L. Simone, F. Loiacono, M. Svelto, F. Benfenati, Role of pericytes in blood–brain barrier preservation during ischemia through tunneling nanotubes, Cell Death Dis. 13 (2022), https://doi.org/10.1038/s41419-022-05025-y.
[61] A. Daina, V. Zoete, A boiled-egg to predict gastrointestinal absorption and brain penetration of small molecules, ChemMedChem (2016) 1117–1121, https://doi.org/10.1002/cmdc.201600182.
[62] A.H. Schinkel, P-Glycoprotein, a Gatekeeper in the blood-brain Barrier, 1999.
[63] Schrödinger Release 2020-4: Maestro, 2020.
[64] Schrödinger Release 2020-4: Ligprep, 2020.
[65] R.C. Johnston, K. Yao, Z. Kaplan, M. Chelliah, K. Leswing, S. Seekins, S. Watts, D. Calkins, J. Chief Elk, S.V. Jerome, M.P. Repasky, J.C. Shelley, Epik: pka and protonation State prediction through machine learning, J. Chem. Theor. Comput. 19 (2023) 2380–2388, https://doi.org/10.1021/acs.jctc.3c00044.
[66] J.L. Banks, H.S. Beard, Y. Cao, A.E. Cho, W. Damm, R. Farid, A.K. Felts, T. A. Halgren, D.T. Mainz, J.R. Maple, R. Murphy, D.M. Philipp, M.P. Repasky, L. Y. Zhang, B.J. Berne, R.A. Friesner, E. Gallicchio, R.M. Levy, Integrated Modeling Program, Applied Chemical Theory (IMPACT), J. Comput. Chem. 26 (2005) 1752–1780, https://doi.org/10.1002/jcc.20292.
[67] H.M. Berman, J. Westbrook, Z. Feng, G. Gilliland, T.N. Bhat, H. Weissig, I. N. Shindyalov, P.E. Bourne, The protein data bank. http://www.rcsb.org/pdb/status.html, 2000.
[68] J. Reis, N. Manzella, F. Cagide, J. Mialet-Perez, E. Uriarte, A. Parini, F. Borges, C. Binda, Tight-binding inhibition of human monoamine oxidase B by chromone analogs: a kinetic, crystallographic, and biological analysis, J. Med. Chem. 61 (2018) 4203–4212, https://doi.org/10.1021/acs.jmedchem.8b00357.
[69] H. Berman, K. Henrick, H. Nakamura, Announcing the worldwide protein data bank, Nat. Struct. Mol. Biol. 10 (2003), https://doi.org/10.1038/nsb1203-980, 980–980.
[70] Schrödinger Release 2020-4: Protein Preparation Wizard, 2020.
[71] A.E. Cho, V. Guallar, B.J. Berne, R. Friesner, Importance of accurate charges in molecular docking: Quantum Mechanical/Molecular Mechanical (QM/MM) approach, J. Comput. Chem. 26 (2005) 915–931, https://doi.org/10.1002/jcc.20222.
[72] Schrödinger Release 2020-4: Glide, 2020.
[73] S. Genheden, U. Ryde, The MM/PBSA and MM/GBSA methods to estimate ligand-binding affinities, Expet Opin. Drug Discov. 10 (2015) 449–461, https://doi.org/10.1517/17460441.2015.1032936.
[74] F. Mohamadi, N.G.J. Richards, W.C. Guida, R. Liskamp, M. Lipton, C. Caufield, G. Chang, T. Hendrickson, W.C. Still, Macromodel—An integrated software system for modeling organic and bioorganic molecules using molecular mechanics, J. Comput. Chem. 11 (1990) 440–467, https://doi.org/10.1002/jcc.540110405.

[75] G.D. Marconi, L. Fonticoli, T.S. Rajan, P. Lanuti, Y. Della Rocca, S.D. Pierdomenico, O. Trubiani, J. Pizzicannella, F. Diomede, Transforming growth Factor-Beta1 and human gingival fibroblast-to-myofibroblast differentiation: molecular and morphological modifications, Front. Physiol. 12 (2021), https://doi.org/10.3389/fphys.2021.676512.

[76] G.D. Marconi, M. Gallorini, S. Carradori, P. Guglielmi, A. Cataldi, S. Zara, The up-regulation of oxidative stress as a potential mechanism of novel MAO-B inhibitors for glioblastoma treatment, Molecules 24 (2019), https://doi.org/10.3390/molecules24102005.

[77] G.D. Marconi, Y. Della Rocca, L. Fonticoli, S. Guarnieri, S. Carradori, T. Soundara Rajan, J. Pizzicannella, F. Diomede, The beneficial effect of carvacrol in HL-1 cardiomyocytes treated with LPS-G: Anti-inflammatory pathway investigations, Antioxidants 11 (2022), https://doi.org/10.3390/antiox11020386.

[78] G.D. Marconi, S. Carradori, A. Ricci, P. Guglielmi, A. Cataldi, S. Zara, Kinesin Eg5 targeting inhibitors as a new strategy for gastric adenocarcinoma treatment, Molecules 24 (2019), https://doi.org/10.3390/molecules24213948.